



ELSEVIER

Contents lists available at ScienceDirect

Precision Engineering

journal homepage: www.elsevier.com/locate/precision

A multiobjective optimization model for machining quality in the AISI 12L14 steel turning process using fuzzy multivariate mean square error

Juliana Helena Daroz Gaudêncio^{a,*}, Fabrício Alves de Almeida^a, João Batista Turrioni^a, Roberto da Costa Quinino^b, Pedro Paulo Balestrassi^a, Anderson Paulo de Paiva^a

^a Institute of Industrial Engineering and Management, Federal University of Itajubá, Itajubá, MG, 37500-903, Brazil

^b Department of Statistics, Federal University of Minas Gerais, Belo Horizonte, MG, 31270-901, Brazil

ARTICLE INFO

Keywords:

Robust parameter design
Normal boundary intersection
Principal components analysis
Fuzzy decision maker

ABSTRACT

Organizations focus on determining optimal operating conditions to ensure quality; however, industrial processes exhibit a high degree of variability and the use of robust estimators is a suitable alternative to model experimental data. As a case study, the surface roughness (R_a) of an AISI 12L14 steel turning process is optimized to find a centrality measure close to its target with minimum dispersion and thus improve the quality of the machined surface by choosing the best values of the associated parameters. The main contribution of this research is the proposal of a multiobjective optimization method that uses principal components analysis to minimize the redundancy of objective functions in terms of multivariate mean square error, thus making optimization of the process possible with a better explanation of all centrality and dispersion estimators proposed herein. The method uses a fuzzy decision maker to show the surface roughness' optimum result with the most efficient production taken into consideration. To prove its efficiency, confirmation runs were conducted. At a confidence level of 95%, the optimal value falls within the multivariate confidence intervals only for Model B, in which the estimators' median and median absolute deviation are considered, thus affirming which pair of estimators achieves the most robust parameter design solution. Through the proposed research, the developed model can be used in industries for determining machining parameters to attain high quality with minimum power consumption and hence maximum productivity.

1. Introduction

Organizations that try to focus on optimum operating conditions must ensure quality and continuously search for improvements. They aim at minimizing the uncertain measurements that provide variation and affect accuracy. Measurement uncertainties affect the responses (y) and also the predictor variables (x); therefore, it is reasonable to use robust analysis tools to minimize these effects. In that scope, the design of experiments (DOE) approach is a particularly excellent tool for optimizing certain process quality characteristics [1]. Many researchers have applied the response surface methodology (RSM), in which one aims to discern answers that are influenced by some variables to optimize results. The principal objective is to obtain an adequate model from a sequence of designed experiments to obtain optimal operating conditions for the process [2,3].

Experimentation directs the development and improvement of existing processes and facilitates the development of robust processes that are minimally affected by variation of external agents. The processes

that produce minimal variation in the presence of noise fall under the category of robust parameter design (RPD), which is an engineering methodology intended to be a cost-effective approach to improving product quality [4].

RPD was allied with the RSM approach by Myers and Carter [5]. They were aiming to solve problems in which the experimenter was able to identify a primary response to be optimized by being limited to a specific value of average or variance as the secondary response. This idea was popularized by Vining and Myers [6], who pointed out that the objective of optimizing the mean $\hat{\mu}(x)$ and variance $\hat{\sigma}^2(x)$ simultaneously could be achieved through the dual-response surface method.

Consequently, estimators of mean and variance are normally used. Industrial processes, however, often exhibit high variability in repeated observations. This approach raises a question pointed out by Boylan and Cho [7]: Which robust estimators achieve the best RPD solutions? Therefore, in this work, we compare eight dual-response surface models to define the best. The first model (Model A) comprises a sample mean

* Corresponding author.

E-mail addresses: juliana_hdg@yahoo.com.br, ju.gaudencio@gmail.com (J.H. Daroz Gaudêncio).

<https://doi.org/10.1016/j.precisioneng.2019.01.001>

Received 4 October 2018; Received in revised form 21 December 2018; Accepted 7 January 2019

0141-6359/ © 2019 Elsevier Inc. All rights reserved.

Table 1
Combination of estimators used in comparative analysis.
Source: Adapted from Boylan and Cho [7].

Model	Location estimators	Scale estimators
A	Sample mean (\bar{x})	Standard deviation (s)
B	Median (\bar{x})	Median absolute deviation
C	Huber's Proposal 2 (\bar{x}_{H2})	Huber's Proposal 2 (S_{H2})
D	Hodges–Lehmann estimator (HL_n)	S_n estimator
E	Hodges–Lehmann estimator (HL_n)	Q_n estimator
F	Tau (\bar{x}_τ)	Tau (s_τ)
G	Hodges–Lehmann estimator (HL_n)	Median absolute deviation
H	Maximum likelihood estimator (\bar{x}_{MLE})	Maximum likelihood estimator (s_{MLE})

and standard deviation and the remaining models (B–H) comprise the nonparametric estimators as described in Table 1.

These eight dual-response surface models were grouped through a principal components analysis (PCA) that solves the dependence and neutralizes the effects of the correlation coefficients of multiple objective functions and also enables a dimensionality reduction in the number of objective functions [8]. The approach proposed herein involves calculations of a dataset covariance matrix to minimize redundancy and thus make it possible to optimize the process with a better explanation of estimators.

The optimization proposed applies an algorithm to the principal component scores originated by centrality and dispersion objective functions. The next step is to optimize the scores through the multivariate mean square error (MMSE) that combines the techniques of RSM and PCA for multiobjective optimization problems and considers the correlation structure among answers. The idea is to determine the vectors of decision variables that simultaneously satisfy functions and restrictions to find an acceptable value for each response [9]. To complete the proposal, the normal boundary intersection (NBI) method is chosen to construct a convex and equispaced Pareto frontier capable of obtaining a feasible set of solutions [10]. A fuzzy decision maker (DM) then provides the best solution of process input parameters to improve the manufacturing process.

Therefore, in our multiobjective optimization, we implement the algorithm on the AISI 12L14 steel turning process with an ISO P35 hard metal tool [11], using a crossed array. The data address the influence of control and noise variables. This case study was performed in a central composite design (CCD) with three input/control factors: cutting speed (V_c), cutting feed (f_n), and machining depth (a_p); also considered as noise variables are piece slenderness (z_1), tool flank wear (z_2), and measurement position (z_3) evaluation as a response to sample surface roughness, R_a . Accordingly, the proposed algorithm determines the setup of the turning process control/input parameters that are capable of achieving reduced surface roughness with minimal variance.

Analogously, by considering the noises (z_1) and (z_3), this work will address the following research issue: ensuring that the piece roughness is the same throughout its length despite the measurements not being stationary. Two critical objectives in surface tool path optimization are machining accuracy and process efficiency and thus providing a surface machining error. In order to determine optimal tool path parameters that will simultaneously satisfy the tradeoff incurred between these objectives, techniques of optimization are presented [12,13].

Also, making the optimum choice of cutting parameters and tool path design can save ~6%–40% in the energy used in mechanical processes, which are widely used in the manufacturing industry and consume more energy than any other industrial process [14]. The operational ranges of cutting parameters must not negatively impact the quality of machined parts, material removal rate, or productivity.

This paper is organized as follows: Section 2 presents a theoretical reference for nonparametric estimators that can be used to model the roughness and thus provides a problem with multiple responses. The

explanation of problem dimensionality reduction is described in Section 3. Section 4 presents the proposed algorithm used to solve multi-objective problems. Problem resolution and a discussion of numerical results are detailed in Section 5. Finally, Section 6 includes some conclusions and extensions.

2. Nonparametric estimators

It is known, in most cases, that the responses of a dynamic process are difficult to measure, which motivates the exploration of effective robust estimators. In this case, the robust term describes the ability an estimator has to overcome the outliers' impact on the process estimate responses [15].

The main objective of robust design is to obtain the optimum conditions of input variables to minimize the variability associated with the quality characteristic analyzed in the process while also keeping the process mean at the target value. In this context [16], the response surface approach uses the ordinary least squares method to obtain adequate response functions for the process mean and variance under the assumptions that the experimental data are normally distributed and that there is no major contamination in the data set. However, these assumptions may not hold in modeling many real-world industrial problems. The sample mean and variance are efficient under the normal distribution, but they are very sensitive to contamination or departures from the normality assumption. To remedy this problem, we propose modeling the data set by efficient and outlier-resistant estimators as detailed in Table 1.

2.1. Comparative study among robust estimators

The robust estimators are compared according to the following properties [17,18]: (1) the breakdown point, which represents the maximum fraction of outliers that can be added to a given sample without spoiling the data estimate, and (2) the relative efficiency, which is assigned to the normality. The breakdown point cannot exceed the value of 50% because, if more than half of the observations are contaminated, it is not possible to distinguish between the subjacent and contaminated distributions [17].

2.1.1. Median and median absolute deviation

The median is characterized as a measure of central tendency and offers the advantage of being very insensitive to the presence of outliers [19]. According to Rousseeuw and Croux [20], the median absolute deviation (MAD) is characterized as a very robust scale estimator that has been researched [21] and was discovered and popularized by Hampel [22]. If $x = (x_1, x_2, \dots, x_n)$ is a data set, then the sample median is defined by

$$MAD = b \cdot \text{med}_i |x_i - \text{med}_j x_j| \quad (1)$$

The constant b in Eq. (1) is set to the value $b = 1.4826$ to relate the normality assumption and thereby disregard the abnormality induced by outliers. Both the median and the MAD have a breakdown point of 50% which is the highest possible. This characteristic is related to how strongly the outliers have an effect; however, these measure are also well known for their comparative lack of efficiency under normality, being 64% and 37% for each, respectively [23].

2.1.2. S_n and Q_n scale estimators

Rousseeuw and Crox [23] proposed two scale estimators with breaking points of 50% but that are more efficient than the MAD. The first is S_n , which has a relative efficiency equal to 58% (superior to that of the MAD) and as defined by

$$S_n = c_n \cdot 1.1926 \text{med}_i \{ \text{med}_j |x_i - x_j| \} \quad (2)$$

The other estimator proposed is Q_n , which shares the same attractive properties of the S_n estimator, has a break point of 50%, is also

appropriate for asymmetric distributions, and has a very high relative efficiency of ~82%. Furthermore, it has a simple and explicit formula:

$$Q_n = d_n \cdot 2,2219 \{|x_i - x_j|; i < j\} \quad (3)$$

2.1.3. HL_n location estimator

The HL_n location estimator is an estimator proposed by Hodges and Lehmann [24] and it is known for its excellent overall performance in terms of efficiency and resistance in relation to outliers. This location estimator has the relative efficiency of ~86% and thus is highly competitive with the mean under the normal distribution, although it has a break point of 29% [25]. If $x = (x_1, x_2, \dots, x_n)$ is a data set where the estimator is obtained by the median of all pairwise averages, then HL_n is defined by

$$HL_n = \text{med}\left\{\frac{x_i + x_j}{2}\right\} \quad (4)$$

2.1.4. Huber's proposal 2 estimators

Lee et al. [16] investigated the M-estimation approach proposed by Huber [26] as a highly efficient alternative to the median and the MAD. Huber's Proposal 2 M-estimators have a high efficiency; the location estimator has a relative efficiency of 96% and the scale estimator has an efficiency of 80%. Huber [27] proposed the simultaneous solution for μ and σ :

$$\sum_{i=1}^n \Psi\left(\frac{x_i + \mu}{\sigma}\right) = 0 \quad (5)$$

$$\sum_{i=1}^n \Psi^2\left(\frac{x_i + \mu}{\sigma}\right) = \eta \quad (6)$$

where the data set is $x = (x_1, x_2, \dots, x_n)$.

2.1.5. Tau estimators

Maronna and Zamar [28] developed tau estimators to reduce the computational complexity and associated times in relation to other robust estimators with a high breaking point. If $x = (x_1, x_2, \dots, x_n)$ is a data set, then the estimators are

$$\tilde{x}_\tau = \frac{\sum_i x_i w_i}{\sum_i w_i} \quad (7)$$

$$s_\tau = \sqrt{\frac{s_0^2}{n} \sum_i \rho_{C2}\left(\frac{x_i - \tilde{x}_\tau}{s_0}\right)} \quad (8)$$

where

$$w_i = W_{C1}\left(\frac{x_i - \text{med}(x)}{s_0}\right); W_c(x_i) = \left(1 - \left(\frac{x_i}{c}\right)^2\right)^2; s_0 = MAD(x); \rho_c(x_i) = \min(x_i^2, c^2) \quad (9)$$

Both estimators combine relatively high efficiency (80% for each) with high resistivity when $c_1 = 4.5$ and $c_2 = 3.0$.

2.1.6. Maximum likelihood estimators

Finally, maximum likelihood estimators (MLE) of location and scale will form the last couple of estimators. They estimate different parameter values of a statistical model to maximize the observed data probability under the assumption of a normal distribution [29]. O'Hagan and Leonard [30] introduced inclined distributions for the MLE because the distribution of a normal inclination is reduced to normal when $\alpha = 0$; the normality becomes a special case of a distribution that makes it possible to model symmetrical and asymmetrical situations. Therefore, numerical parameters are estimated by maximizing the likelihood function with the components $\theta = (\mu, \sigma, \alpha)$ as given by

$$\log L(\theta) = -\frac{k}{2} \log \frac{\pi \sigma^2}{2} - \frac{1}{2\sigma^2} \sum_{i=1}^k (x_i - \sigma)^2 + \sum_{i=1}^k \log \Phi\left[\frac{\alpha(x_i - \mu)}{\sigma}\right] \quad (10)$$

where $x = (x_1, x_2, \dots, x_k)$ is a data set and μ and σ are the location and scale parameters, respectively.

3. Dimensionality reduction

PCA is concerned with explaining the variance–covariance structure of variables set through a few linear combinations. Suppose that the multiple objective functions $f_1(x), f_2(x), \dots, f_p(x)$ are correlated response surfaces written as a random vector $Y^T = [Y_1, Y_2, \dots, Y_p]$. If one assumes that Σ is the variance–covariance matrix associated with this vector, then Σ can be factorized in pairs of eigenvalues–eigenvectors $(\lambda_i, e_i), \dots, (\lambda_p, e_p)$, where $\lambda_1 \gg \lambda_2 \gg \dots \gg \lambda_p \gg \dots$, such that the i th principal component may be stated as $PC_i = e_i^T Y = e_{i1} Y_1 + e_{i2} Y_2 + \dots + e_{ip} Y_p$, with $i = 1, 2, \dots, p$ [31,32].

Analogously, PCA is one of the most frequently used multivariate analysis techniques used to reduce the dimensionality of data sets consisting of a number of correlated variables while retaining as much of the variation as possible [33]. This technique uses an orthogonal transformation to convert the set of observations into a new set of uncorrelated variables. The number of principal components is less than or equal to the number of original variables, and the first few principal components retain most of the variation present in all of the data set [34]. To identify the k significant principal components, one uses Kaiser's criteria, where only those principal components whose eigenvalues are > 1 should be retained to represent the original variables. Furthermore, the k principal components may accumulate at least 80% of variance [31].

PCA can be derived from multivariate normal random variables, distributed as $N_p(\mu, \Sigma)$. The density of random variable Y is constant on the μ centered ellipsoid such as

$$(y - \mu)' \Sigma^{-1} (y - \mu) = c^2 \quad (11)$$

Equation (11) is an ellipse equation centered at the mean vector with half-axes equal to $\pm c \sqrt{\lambda_i} e_i, i = 1, 2, \dots, p$, where (λ_i, e_i) represents the eigenvalue–eigenvector pairs of Σ . In terms of eigenvalues and eigenvectors of the covariance matrix, it may be written as

$$\begin{aligned} y^T [\Sigma_y^{-1}] y &= \left(\frac{y_1}{\sqrt{\sigma_{11}}}\right)^2 + \left(\frac{y_2}{\sqrt{\sigma_{22}}}\right)^2 = y^T \left[\frac{e_1 e_1^T}{\lambda_1} + \frac{e_2 e_2^T}{\lambda_2}\right] y \\ &= \frac{(y^T e_1)^2}{\lambda_1} + \frac{(y^T e_2)^2}{\lambda_2} = c^2 \end{aligned} \quad (12)$$

A constant-density ellipse and the principal components for a bivariate normal random vector with interval confidence $(1 - \alpha)$ are shown in Fig. 1. Compared to the original variables, principal components will not influence each other owing to their uncorrelated nature, which may greatly improve the efficiency for data analytics [35].

The appropriate way to evaluate numerically the adequacy of a multivariate optimization solution in comparison to mathematical solutions is to build a multivariate confidence interval or a multivariate confidence region. If one supposes there are p characteristics and n confirmation runs and considers that the p th characteristic is normally distributed as $N(\bar{y}_p, s_{pp})$, then the 100 $(1 - \alpha)\%$ multivariate confidence is given by

$$\begin{aligned} \bar{y}_p - \left(\sqrt{\frac{p(n-1)}{n(n-p)} F_{(p,n-p)}(\alpha)}\right) \times \sqrt{\frac{s_{pp}}{n}} &\leq y_p \\ &\leq \bar{y}_p + \left(\sqrt{\frac{p(n-1)}{n(n-p)} F_{(p,n-p)}(\alpha)}\right) \times \sqrt{\frac{s_{pp}}{n}} \end{aligned} \quad (13)$$

This multivariate confidence interval will be used in this work to represent the results of confirmation runs. If the method is effective in

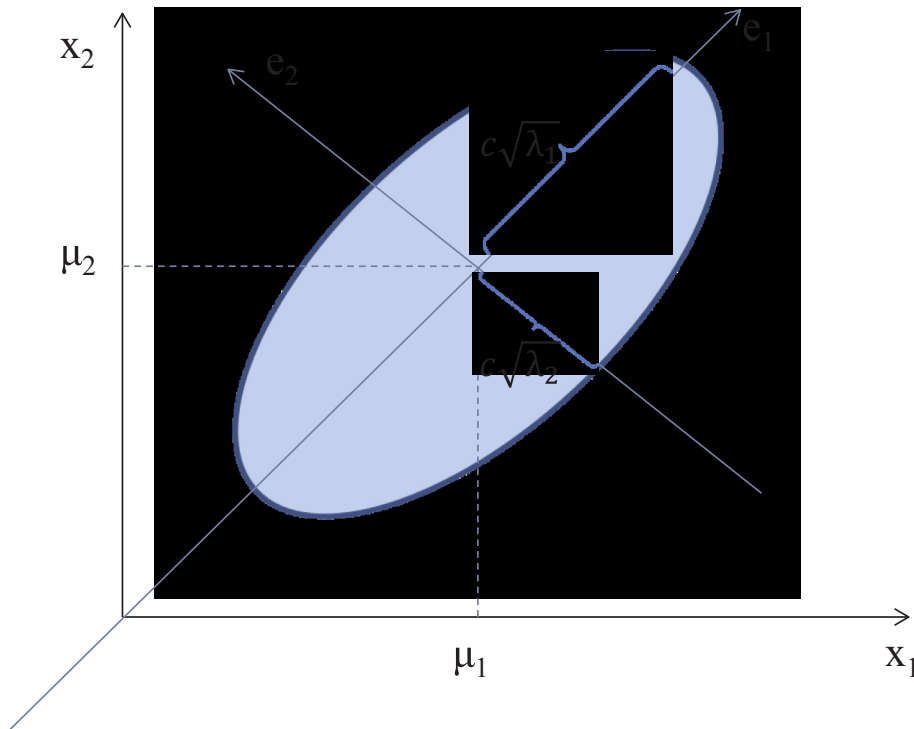


Fig. 1. Constant density ellipse.

finding multiobjective optimization results, then the sample mean of these runs will fall inside the 100 (1- α)% confidence region. Analogously, a two-dimensional confidence ellipse for the mean vector is defined [31] as

$$\begin{bmatrix} y_1(\mathbf{x}_0) \\ y_2(\mathbf{x}_0) \end{bmatrix} = \begin{bmatrix} \bar{y}_1(\mathbf{x}_0) \\ \bar{y}_2(\mathbf{x}_0) \end{bmatrix} + \sqrt{\frac{p(n-1)}{n(n-p)} F_{(p,n-p)}(\alpha)} \times \begin{bmatrix} \sqrt{\lambda_1} & 0 \\ 0 & \sqrt{\lambda_2} \end{bmatrix} \times \begin{bmatrix} e_{11} & e_{12} \\ e_{21} & e_{22} \end{bmatrix} \times \begin{bmatrix} \cos \theta \\ \sin \theta \end{bmatrix} \quad (14)$$

where $0 \leq \theta \leq 2\pi$.

4. Proposed multiobjective optimization

The optimization of multiple process characteristics without consideration of the variance–covariance structure among the responses may lead to an inadequate solution. To treat this constraint, in this section we focus on the MMSE approach [36], which combines the RSM and PCA to address multidimensional nominal-the-best problems. Mathematically, the MMSE can be established as a multivariate dual-response surface, such as

$$\begin{aligned} \text{Minimize } MMSE_T &= [\prod_{i=1}^k (MMSE_i | \lambda_i \geq 1)]^{\frac{1}{k}} \\ &= [\prod_{i=1}^k [(PC_i - \xi_{PC_i})^2 + \lambda_i \lambda_i \geq 1]]^{\frac{1}{k}}; k \leq p \\ \text{subject to } \bar{g}(x) &= x^T x \leq \rho^2 \end{aligned} \quad (15)$$

where

$$\xi_{PC_i} = e_i^T [Z(Y_p | \xi_{Y_p})] = \sum_{j=1}^q \sum_{i=1}^p e_{ij} [Z(Y_p | \xi_{Y_p})] \quad (16)$$

$i = 1, 2, 3, \dots, p; j = 1, 2, 3, \dots, q$

and k is the number of MMSE functions according to the significant principal components, PC_i is the fitted second-order polynomial, ξ_{PC_i} is the target value of the i th principal component that must keep a direct relation with the targets established for the original dataset, $\bar{g}(x)$ is the experimental region constraint, e_i represents the eigenvector set

associated with the i th principal component, and ξ_{Y_p} represents the target for each of the p original responses.

Multiple correlated responses agglutinated in terms of principal component scores and then optimized by using the MMSE approach have the objective of obtaining the Pareto optimal solutions for a bi-objective frontier. In this scenario, the NBI method [10] is applied to find a uniform distribution of Pareto optimal solutions for nonlinear multiobjective problems. Also, it compensates for the shortcomings attributed to other methods because the NBI method is independent of the functions' relative scales and is successful in producing an evenly distributed set of points [9]. Other research in which optimization techniques have been developed to improve manufacturing processes can be seen in Refs. [37,38].

4.1. NBI method

The first step in the NBI method [10] comprises establishment of the payoff matrix Φ that represents the optimal values of each objective function minimized individually as represented by

$$\Phi = \begin{bmatrix} f_1^*(x_1^*) & f_1(x_2^*) & \dots & f_1(x_k^*) \\ f_2(x_1^*) & f_2^*(x_2^*) & \dots & f_2(x_k^*) \\ \vdots & \vdots & \ddots & \vdots \\ f_k(x_1^*) & f_k(x_2^*) & \dots & f_k^*(x_k^*) \end{bmatrix} \quad (17)$$

where x_i^* is the vector of variables that minimizes the i th objective function $f_i(x)$ individually, $f_i^*(x_i^*)$ is the minimum value of objective function f_i , and $f_j(x_i^*)$ is the value of objective function f_j evaluated for a solution that minimizes the function f_i . Through Φ , it is also possible to define some important points such as the Utopia (f^U) and Nadir points (f^N) that represent the minimum and maximum values of f_i , respectively.

Accordingly, the NBI formulation for a bidimensional problem can be described as

$$\text{Minimize } \bar{f}_1(x) \quad (18)$$

$$\text{subject to } \bar{g}_1(x) = \bar{f}_1(x) - \bar{f}_2(x) + 2w - 1 = 0$$

$$\bar{g}_2(x) = x^T x \leq \rho^2$$

$$0 \leq w \leq 1$$

where w are weights that establish the trade-off relationship between $\bar{f}_1(x)$ and $\bar{f}_2(x)$ and where ρ is the radius of the spherical experimental region of the turning process. Because $\bar{f}_1(x)$ and $\bar{f}_2(x)$ are scalarized objective functions, they can be represented as

$$\bar{f}_1(x) = \frac{f_1(x) - f_1^U}{f_1^N - f_1^U} \quad (19)$$

$$\bar{f}_2(x) = \frac{f_2(x) - f_2^U}{f_2^N - f_2^U} \quad (20)$$

By considering $f_i(x) = MMSE_i(x)$, $f_i^U = MMSE_i^U(x)$, and $f_i^N = MMSE_i^N(x)$ to develop the scalarization described in Eqs. (19) and (20), a bidimensional NBI method can be rewritten as

$$\begin{aligned} & \text{Minimize } \bar{f}_1(x) = \left(\frac{MMSE_1(x) - MMSE_1^U(x)}{MMSE_1^N(x) - MMSE_1^U(x)} \right) \\ & \text{Subject to } \bar{g}_1(x) = \left(\frac{MMSE_1(x) - MMSE_1^U(x)}{MMSE_1^N(x) - MMSE_1^U(x)} \right) - \left(\frac{MMSE_2(x) - MMSE_2^U(x)}{MMSE_2^N(x) - MMSE_2^U(x)} \right) + 2w \\ & \quad -1 = 0 \\ & \quad \bar{g}_2(x) = x^T x \leq \rho^2 \\ & \quad 0 \leq w \leq 1 \end{aligned} \quad (21)$$

In sequence, the optimization problem in this study can be solved for different weights (w) and thus create an evenly distributed Pareto frontier.

4.2. Fuzzy multivariate mean square error

After the Pareto set is obtained, the most desired solution concerning the roughness surface must be chosen by means of a fuzzy DM that calculates a linear membership function for each objective function in every Pareto optimal solution [39]. Within all of the nondominated and feasible solutions available on the frontier, some solutions may be more appropriate than others. The best solution may be found by following a fuzzy criterion [40,41] using a linear membership, such as

$$\mu_i = \begin{cases} 1, & MMSE_i \leq MMSE_i^U \\ \frac{MMSE_i^N - MMSE_i}{MMSE_i^N - MMSE_i^U}, & MMSE_i^U < MMSE_i < MMSE_i^N \\ 0, & MMSE_i \geq MMSE_i^N \end{cases} \quad (22)$$

where $MMSE_i^U$ and $MMSE_i^N$ correspond to the Utopia and Nadir points, respectively. The values obtained through Eq. (22) suggest how far a nondominated solution satisfies the f_i objective. Thereby, the total membership function of each Pareto optimal solution is computed by considering the individual membership functions and their relative importance (w_i) such as

$$\mu^T = \sum_{n=1}^i w_i \mu_i \quad (23)$$

The better solution is the one has the highest value of the total membership function (μ^T) as close to its respective Utopia.

5. Research development

To achieve the goal of this research, an AISI 12L14 steel turning process is defined as the case study (Fig. 2). It was performed with a set of 17 experiments on a computer numerical control (CNC) lathe (Nardini model Logic 175) with numerical control provided by a CNC MCS 500, having a power of 7.39 HP, and with a maximum rotation spindle of 4000 rpm. The cutting tool used is the hard metal of class ISO P35 coated with three covers (Ti (C, N), Al₂O₃, and TiN), (GC 4035 Sandvik

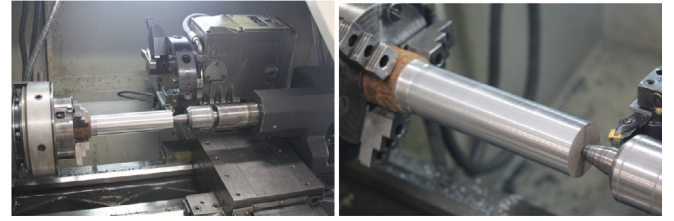


Fig. 2. AISI 12L14 turning process.

Table 2
Control variables and respective levels.

Control variables	Unit	Symbol	Level		
			-1	0	+1
Cutting speed	m/min	V_c	220	280	340
Cutting feed	mm/rev	f	0.08	0.10	0.12
Machining depth	mm	d	0.70	0.95	1.20

of geometry ISO SNMG 09 03 04 – PM. To illustrate the proposed research, the work is developed through the following 8 steps as detailed in Fig. 5.

Step 1: Collect the AISI 12L14 steel turning process data set collected from a set of 17 experiments using a central composite design (CCD) with three parameters (V_c , f , and a_p) at two levels ($2^k = 2^3 = 8$), six axial points ($2^k = 6$), and three center points. These parameters strongly influence whether good results are obtained in the turning process in terms of the product's surface finish. The adopted value for the axial distance α was 1.682. The experimental planning was performed at three different levels of input parameters as listed in Table 2. Also, the noise variables with their respective levels are given in Table 3.

The output variable represents the workpiece surface roughness, defined as R_a (the arithmetic mean value of roughness profile's deviations from the mean line within the measurement length). To determine the roughness value of each workpiece in three regions (Fig. 3(a)) a MITUTOYO Surftest SJ-201P rugosimeter was used. A total of 68 workpieces were machined and 12 measuring points each were identified (4 measurement points 90° distant from each other relative to a cross section) in each of the three measuring regions. For each of the 12 measured points, the measurement was made three times and thus each combination of noise gave a calculated mean value.

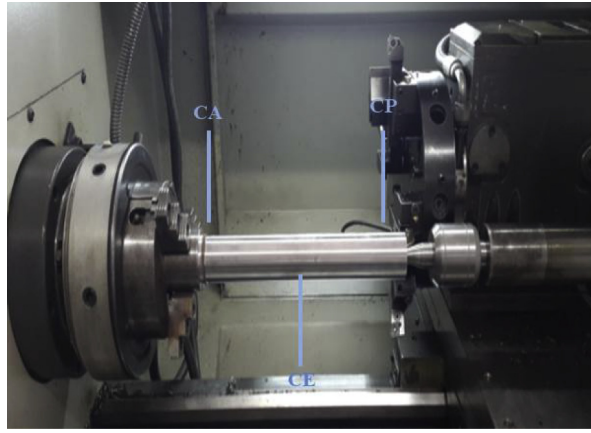
Table 4 lists the R_a experimental data obtained through a cross-over arrangement in which 12 noise conditions were taken into account. These noise conditions provide the non-normality of the data and thus provide the variation with extreme points as shown in Fig. 4; this time series is not stationary and therefore the mean is no longer appropriate. Consequently, the scenario emphasizes the use of robust estimators to model the data.

Step 2: The experimental data are modeled by the location and scale estimators as listed in Table 1. As a result, Table 5 gives the values obtained through the estimators with the 12 noise conditions taken into account.

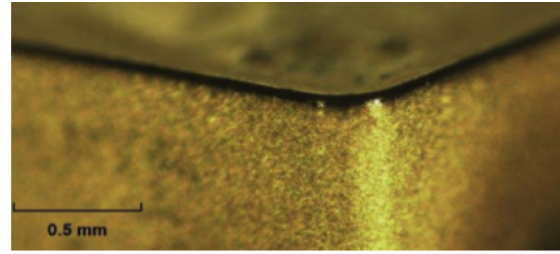
Step 3: To verify whether there is a dependence relationship among

Table 3
Noise variables and respective levels.

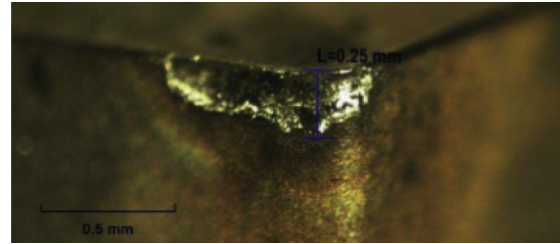
Noise variables	Unit	Symbol	Level		
			-1	0	+1
Workpiece diameter	mm	ϕ	50	–	30
Tool flank wear	mm	VB	0.0	–	0.3
Measurement position	–	P	CP	CE	CA



(a)



(b)



(c)

Fig. 3. (a) Distribution of measurement points in each workpiece, (b) New tool edge ISO P35, and (c) Wear tool edge ISO P35 [42].

the responses detailed in Table 5, a cluster analysis of these multiple responses was performed. A dendrogram was obtained with the correlation distance measure through the Ward linkage method as shown in Fig. 6. Therefore, the 13 original responses are separated into two clusters: Cluster 01 (\bar{x} , s , \bar{x}_{MLE} , and s_{MLE}) and Cluster 02 (\bar{x} , MAD , \bar{x}_{H2} , s_{H2} , HL_n , S_n , Q_n , \bar{x}_τ , and S_τ).

Step 4: As the dependence of multiple responses is confirmed, PCA can be applied. Using the correlation matrix, principal component scores must be extracted and stored with the respective eigenvalues and eigenvectors of the original responses. Table 6 lists the relevant principal component scores that represent the original responses.

Step 5: With the significant principal components that represent the original responses defined, the ordinary least squares (OLS) method is applied to estimate the coefficients of a second-order polynomial according to the response surface methodology. A full quadratic model of each principal component is obtained as shown in the following

equations:

$$PC_1C_1 = 1.596 + 0.336V_c - 0.646f + 1.185a_p - 0.293V_c^2 - 0.963f^2 - 0.732a_p^2 + 0.457V_c f + 0.020V_c a_p - 0.910f a_p \quad (24)$$

$$PC_1C_2 = 3.3711 + 0.803V_c - 1.138f + 0.444a_p - 1.891V_c^2 - 1.721f^2 - 1.007a_p^2 + 0.603V_c f + 0.225V_c a_p - 0.685f a_p \quad (25)$$

$$PC_2C_2 = 0.234 + 0.238V_c - 1.023f - 0.621a_p + 0.0591V_c^2 - 0.185f^2 - 0.166a_p^2 - 0.129V_c f + 0.209V_c a_p + 0.188f a_p \quad (26)$$

Figs. 7–9 show the response surfaces in terms of process parameters that illustrate the quadratic models detailed in Eqs. (24)–(26).

Step 6: After the conclusion of the modeling stage, the optimization is then applied. However, before starting the optimization, it is necessary to define the $MMSE_i$ object functions as represented in Eq. (15).

Table 4
R_a experimental data.

k	Noise conditions														
	1	2	3	4	5	6	7	8	9	10	11	12			
Workpiece diameter [mm]	-1	-1	-1	-1	-1	-1	+1	+1	+1	+1	+1	+1			
Tool flank wear [mm]	-1	-1	-1	+1	+1	+1	-1	-1	-1	+1	+1	+1			
Measurement position	-1	0	+1	-1	0	+1	-1	0	+1	-1	0	+1			
i	V _c [m/min]	f [mm/rev]	d [mm]	\bar{x}_{ij1}	\bar{x}_{ij2}	\bar{x}_{ij3}	\bar{x}_{ij4}	\bar{x}_{ij5}	\bar{x}_{ij6}	\bar{x}_{ij7}	\bar{x}_{ij8}	\bar{x}_{ij9}	\bar{x}_{ij10}	\bar{x}_{ij11}	\bar{x}_{ij12}
1	220	0.08	0.70	0.79	0.86	0.83	1.53	1.78	2.32	3.83	0.98	1.05	0.87	0.75	0.78
2	340	0.08	0.70	0.73	0.75	0.80	1.36	2.06	2.25	3.97	1.03	1.02	3.14	1.87	0.85
3	220	0.12	0.70	1.09	1.16	1.17	1.84	2.30	2.15	3.51	1.41	1.48	1.80	1.74	1.74
4	340	0.12	0.70	1.16	1.15	1.26	1.87	2.56	2.43	1.57	1.50	1.49	3.28	1.83	1.98
5	220	0.08	1.20	1.14	1.36	1.26	1.30	1.59	2.11	9.60	1.47	1.69	2.24	1.38	1.45
6	340	0.08	1.20	1.17	0.95	0.90	1.47	1.42	1.80	4.18	1.44	1.60	7.15	3.15	1.31
7	220	0.12	1.20	1.55	1.58	1.59	1.69	1.68	1.73	1.95	1.54	1.58	3.10	2.02	1.87
8	340	0.12	1.20	1.56	1.69	1.62	1.54	1.64	1.65	3.45	1.57	1.62	5.53	3.13	1.81
9	180	0.10	0.95	1.30	1.11	1.13	1.40	1.71	1.53	4.80	1.31	1.37	3.63	1.84	1.65
10	380	0.10	0.95	1.01	0.95	1.04	1.96	1.87	1.74	5.44	1.53	1.41	4.35	2.39	1.36
11	280	0.07	0.95	1.47	1.31	1.33	2.16	2.01	1.87	4.13	2.08	1.26	2.83	1.09	0.66
12	280	0.13	0.95	1.36	1.39	1.46	2.33	2.00	1.92	3.41	1.55	1.52	1.78	1.71	1.73
13	280	0.10	0.53	1.16	1.22	1.27	2.23	2.35	2.49	1.27	1.07	1.10	2.60	1.67	1.76
14	280	0.10	1.37	1.47	1.36	1.40	2.09	2.52	2.49	5.22	1.32	1.26	3.37	2.66	2.51
15	280	0.10	0.95	1.26	1.31	1.42	2.42	2.18	2.20	6.69	1.21	1.20	3.10	2.78	2.06
16	280	0.10	0.95	1.14	1.30	1.32	2.19	2.29	2.29	6.28	1.16	1.14	2.79	3.01	1.96
17	280	0.10	0.95	0.93	0.99	1.15	2.53	2.41	2.37	6.06	1.15	1.18	3.20	2.99	3.62

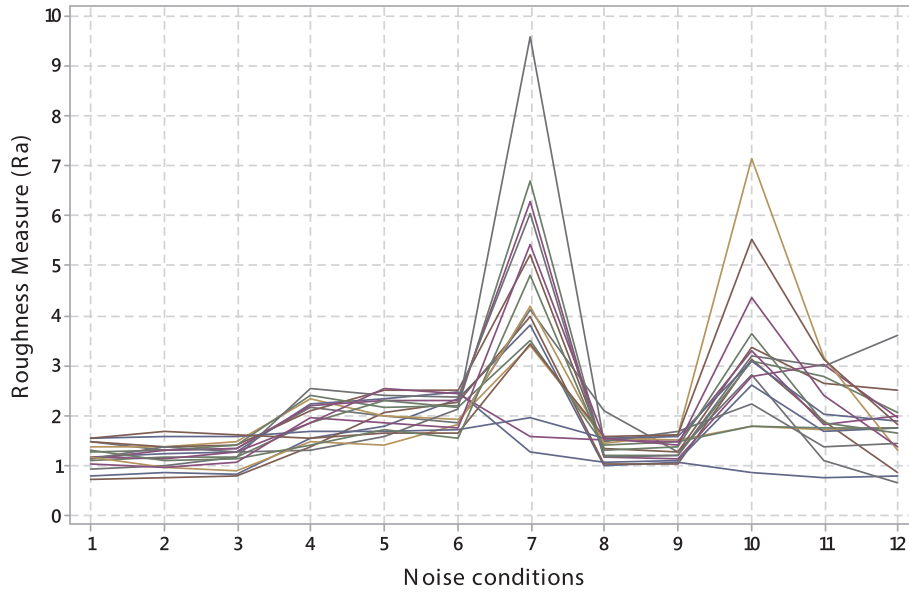


Fig. 4. R_a experimental data with noise conditions.

The MMSE method is used to minimize all the original responses simultaneously with their respective targets expressed in terms of principal components.

The chosen component for Cluster 01 is PC_1C_1 , as detailed in Eq. (24), and its respective MMSE objective function can be expressed as

$$f_1(x) = MMSE_1^1 = \left[(PC_1C_1 - \xi_{PC_1C_1})^2 + \lambda_{PC_1C_1} \right] \quad (27)$$

with

$$\begin{aligned} \xi_{PC_1C_1} = & e_1 [Z(\bar{x}|\xi_{\bar{x}})] + e_2 [Z(s|\xi_s)] + e_3 [Z(\bar{x}_{MLE}|\xi_{\bar{x}_{MLE}})] \\ & + e_4 [Z(s_{MLE}|\xi_{s_{MLE}})] \end{aligned} \quad (28)$$

where the targets expressed in Eq. (28) are calculated and resulted in $\xi_{PC_1C_1} = -3.546$. $\lambda_{PC_1C_1}$ is the eigenvalue detailed in Table 6 and the (e_i) are their respective eigenvectors.

The same approach is done for Cluster 02, where the $MMSE_i$ object functions are calculated for both principal components, PC_1C_2 and PC_2C_2 . The targets are expressed in terms of principal components and result in $\xi_{PC_1C_2} = -3.935$ and $\xi_{PC_2C_2} = 0.929$ as detailed in

$$\begin{aligned} \xi_{PC_1C_2} = & e_1 [Z(\bar{x}|\xi_{\bar{x}})] + e_2 [Z(MAD|\xi_{MAD})] \\ & + e_3 [Z(\bar{x}_{H2}|\xi_{\bar{x}_{H2}})] + e_4 [Z(s_{H2}|\xi_{s_{H2}})] + e_5 [Z(HL_n|\xi_{HL_n})] \\ & + e_6 [Z(S_n|\xi_{S_n})] + e_7 [Z(Q_n|\xi_{Q_n})] + e_8 [Z(\bar{x}_\tau|\xi_{\bar{x}_\tau})] \\ & + e_9 [Z(S_\tau|\xi_{S_\tau})] \end{aligned} \quad (29)$$

Because Cluster 02 has two $MMSE_i$ functions, $MMSE_1^2$ and $MMSE_2^2$ must be multiplied together according to

$$\begin{aligned} f_2(x) = & MMSE_1^2 \\ = & \left\{ \left[(PC_1C_2 - \xi_{PC_1C_2})^2 + \lambda_1 \right] \cdot \left[(PC_2C_2 - \xi_{PC_2C_2})^2 + \lambda_2 \right] \right\}^{\frac{1}{2}} \end{aligned} \quad (30)$$

Because the objective functions $f_1(x)$ and $f_2(x)$ were defined in terms of the MMSE, the NBI method of optimization is adopted to determine the Pareto optimal solutions. The first step comprises establishment of the payoff matrix Φ and, to execute the individual optimization, the generalized reduced gradient (GRG) algorithm is applied. As a result, the Utopia and Nadir points are represented by

$$\Phi = \begin{bmatrix} 3.823 & 16.314 \\ 5.870 & 3.189 \end{bmatrix} \quad (31)$$

Therefore, it is possible to stagger the objective functions according to Eqs. (27) and (30) for bivariate optimization such as

$$\bar{f}(x) = \begin{cases} \bar{f}_1(x) = \frac{MMSE_1^1(x) - 3.823}{16.314 - 3.823} \\ \bar{f}_2(x) = \frac{MMSE_2^2(x) - 3.189}{5.870 - 3.189} \end{cases} \quad (32)$$

Step 7: Scalarization of the objective functions represented by Eqs. (27) and (30) is performed to conduct the NBI method through application of the GRG algorithm in the system of equation (21). The algorithm runs in 5% increments in the weight range. Therefore, 21 Pareto optimal points are obtained, as detailed in Table 7.

The uncoded values of input parameters (V_c , f , and d) are also detailed in Table 7. It is possible to determine the optimal operational range that can be adopted in the process by considering a minimum variation in the surface roughness (R_a) measures. Fig. 10(a) illustrates a bi-objective Pareto frontier of both functions in terms of the MMSE. The feasible region comprising all the original response surfaces is illustrated in Fig. 11, where the lower and upper limits of responses are as detailed in Table 8.

Although all 21 Pareto solutions can be considered optimal solutions, in manufacturing processes, the purpose is to find a unique optimal point. In this way, one implements the fuzzy DM, where the weighting factors are considered a ratio between the individual membership (μ_i) and the sum of both individual membership functions. Fig. 10(b) shows the result obtained of total membership (μ^T) for R_a and also highlights the better solution, which is the one with the highest value (Table 7). Each Pareto optimal solution achieves its fuzzy DM value that defines a better weight composition; as a result, the highest defined value of μ^T , 95.00% for Cluster 01 and 5.00% for Cluster 02, is used to determine a minimal variation for scale estimators. By using these weights, the optimum result for surface roughness (R_a) is found to be equal to 1.461 with a minimal variation to 0.533. Also, the best process input parameters according to the defined weights are equal to $V_c = 273.853$ [m/min], $f = 0.084$ [mm/rev], and $d = 0.583$ [mm].

Also, the optimized original responses assigned to R_a can be seen in Table 9. These measures of centrality and dispersion were obtained through the NBI optimization and are equivalent to the objective functions $f_1(x)$ and $f_2(x)$ in terms of the MMSE.

Step 8: After the optimal point is defined, confirmation experiments are needed. Therefore, power and sample size capabilities were evaluated to ensure enough power and a large enough sample size to detect

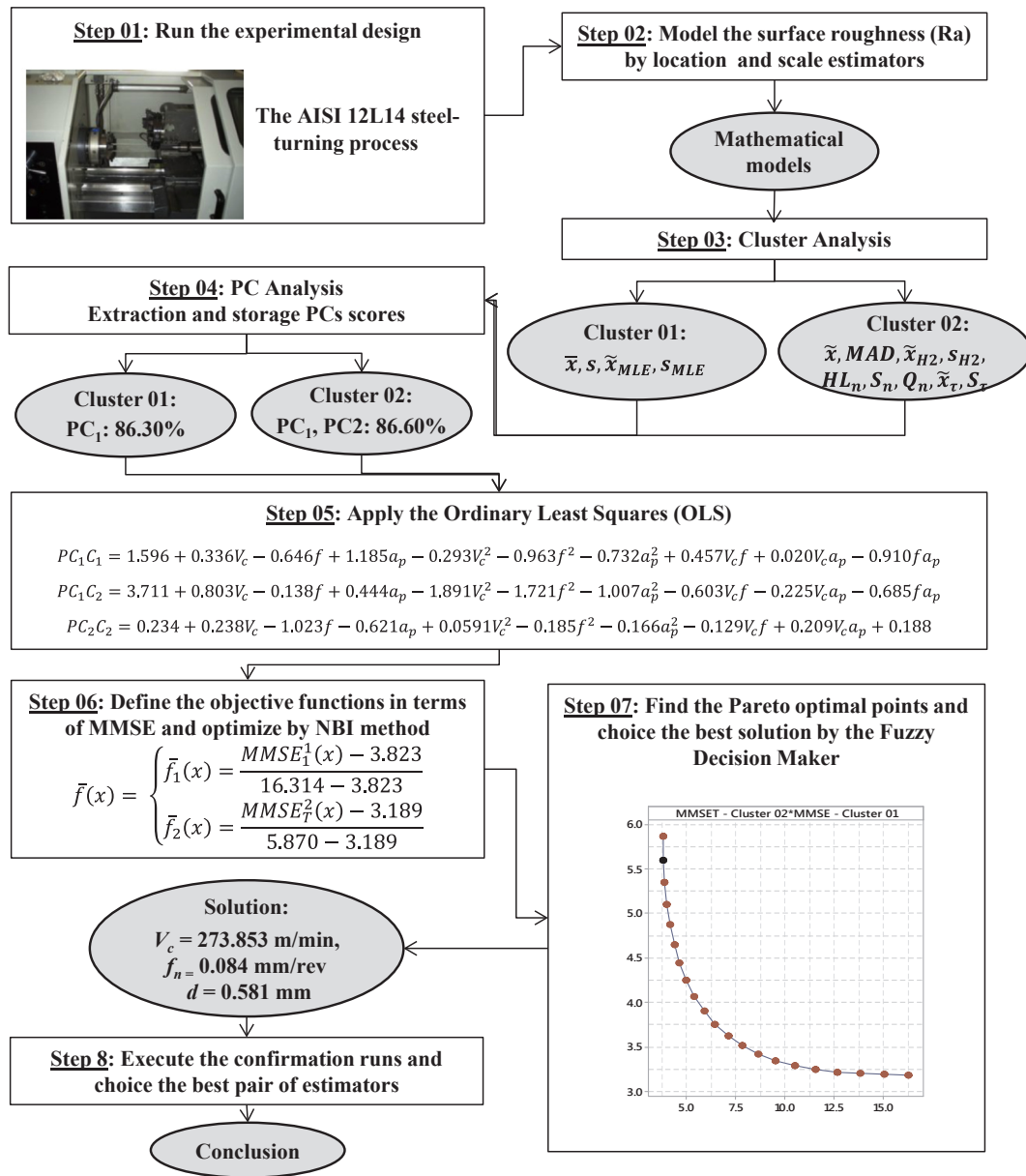


Fig. 5. Development of research methodology.

Table 5

Values obtained for R_a in the modeling by estimators.

\bar{x}	s	\tilde{x}	MAD	\tilde{x}_{H2}	S_{H2}	HL_n	S_n	Q_n	\tilde{x}_τ	s_τ	\tilde{x}_{MLE}	s_{MLE}
1.356	0.923	0.927	0.241	1.192	0.600	1.163	0.282	0.342	0.865	0.306	1.681	0.708
1.648	1.049	1.193	0.668	1.562	0.983	1.496	0.730	0.849	1.189	0.781	1.903	0.890
1.782	0.664	1.740	0.549	1.695	0.514	1.710	0.514	0.550	1.643	0.507	1.881	0.597
1.839	0.643	1.703	0.534	1.792	0.611	1.783	0.682	0.591	1.670	0.559	1.904	0.574
2.220	2.377	1.460	0.266	1.602	0.447	1.534	0.254	0.322	1.417	0.315	3.234	1.593
2.199	1.833	1.455	0.469	1.832	1.086	1.558	0.514	0.614	1.347	0.557	2.620	1.338
1.817	0.431	1.681	0.173	1.728	0.201	1.728	0.158	0.174	1.678	0.184	1.941	0.305
2.235	1.223	1.643	0.115	1.892	0.534	1.704	0.110	0.134	1.628	0.140	2.624	0.822
1.897	1.131	1.465	0.316	1.558	0.411	1.528	0.405	0.402	1.435	0.349	2.290	0.897
2.079	1.406	1.630	0.680	1.759	0.812	1.697	0.777	0.809	1.526	0.728	2.446	1.212
1.846	0.925	1.670	0.607	1.745	0.781	1.707	0.875	1.004	1.616	0.687	1.880	0.844
1.847	0.566	1.721	0.340	1.754	0.370	1.731	0.325	0.351	1.682	0.347	1.945	0.441
1.680	0.586	1.470	0.502	1.680	0.664	1.717	0.674	0.437	1.496	0.600	1.725	0.501
2.301	1.142	2.276	1.245	2.160	0.910	2.047	1.266	1.038	2.098	1.016	2.454	0.904
2.319	1.521	2.118	1.115	2.040	0.870	2.047	1.098	1.077	1.934	0.936	2.852	1.251
2.233	1.433	2.075	1.129	1.986	0.884	2.007	1.148	1.070	1.882	0.949	2.533	1.061
2.257	1.442	2.236	1.505	2.058	1.076	2.071	1.453	1.115	1.979	1.216	2.443	1.158

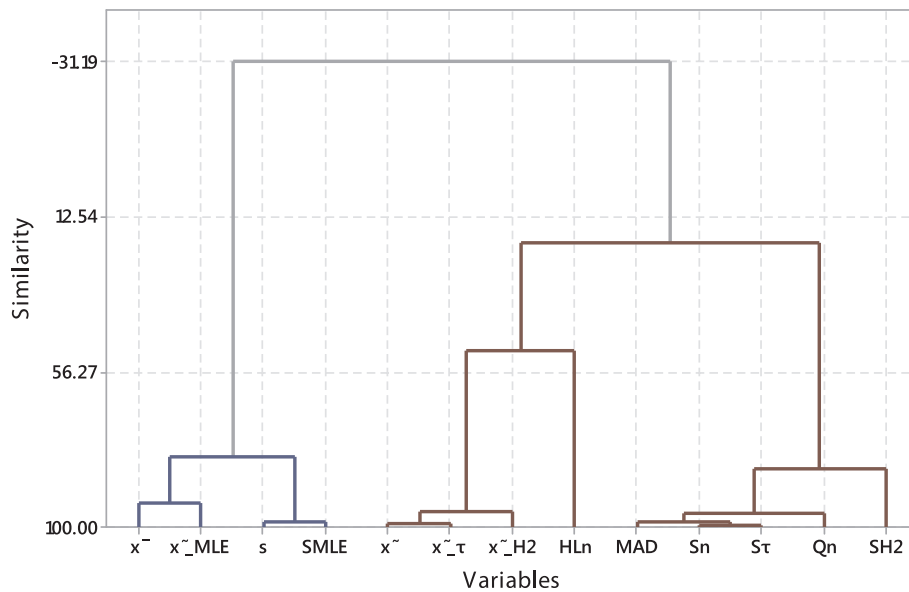


Fig. 6. Hierarchical clustering analysis.

Table 6
Scores of relevant principal components.

k	Cluster 01		Cluster 02
	PC ₁	PC ₁	PC ₂
1	-2.165	-3.969	2.381
2	-1.035	-0.337	2.435
3	-1.654	-0.579	-0.661
4	-1.589	-0.059	-0.578
5	3.836	-2.350	-0.321
6	2.154	-0.319	1.117
7	-2.185	-2.399	-2.067
8	0.855	-2.082	-1.693
9	-0.076	-2.114	-0.174
10	1.138	0.543	0.597
11	-0.930	0.808	0.522
12	-1.797	-1.417	-1.478
13	-2.223	-0.743	0.154
14	0.799	4.176	-1.001
15	2.184	2.836	1.081
16	1.303	3.192	-0.310
17	1.384	4.813	-0.003
Eigenvalue (λ)	3.4524	6.1707	1.6246
Proportion	0.8630	0.6860	0.1810
Cumulative	0.8630	0.6860	0.8660

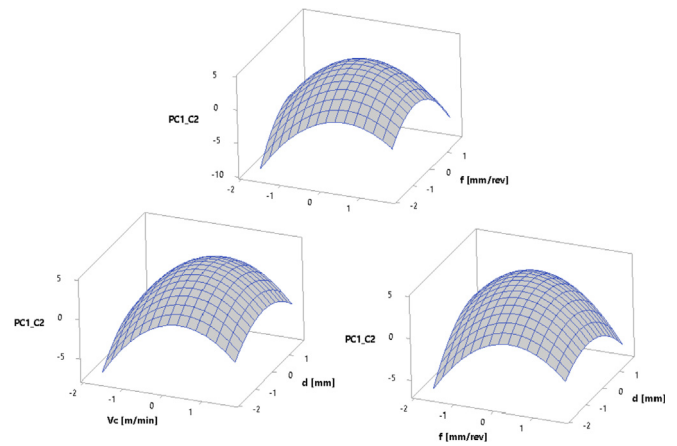


Fig. 8. Response surfaces of PC₁C₂ built in terms of process parameters.

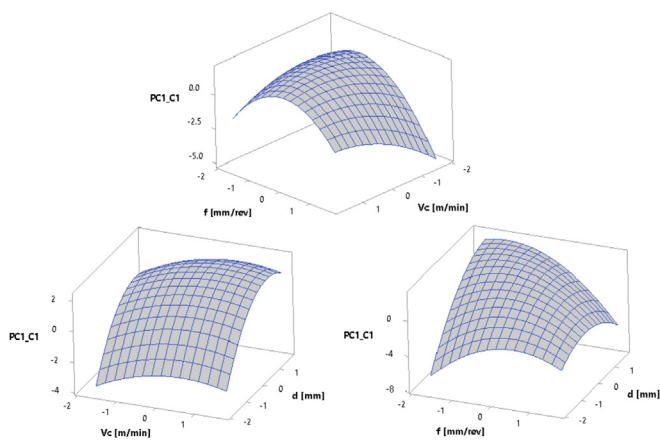


Fig. 7. Response surfaces of PC₁C₁ built in terms of process parameters.

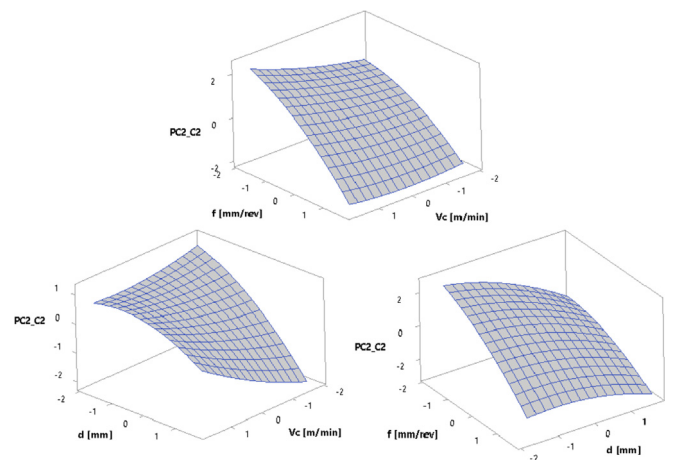


Fig. 9. Response surfaces of PC₂C₂ built in terms of process parameters.

differences of magnitude between the selected optimal points for R_a using the fuzzy NBI-MMSE approach.

At a confidence level of 95%, the one-sample t -test was conducted to confirm whether the optimal value obtained for surface roughness through the proposed optimization algorithm falls within the

Table 7
Pareto optimal solutions for objective functions.

w	Uncoded inputs			$f_1(x) = \text{MMSE}_1^1$	$f_2(x) = \text{MMSE}_2^T$	Fuzzy DM (μ_T)
	V_c [m/min]	f [mm/rev]	d [mm]			
0.00	192.653	0.085	0.845	16.314	3.189	0.050
0.05	191.965	0.087	0.825	15.079	3.192	0.144
0.10	192.006	0.088	0.804	13.875	3.202	0.235
0.15	192.812	0.090	0.783	12.709	3.219	0.324
0.20	194.372	0.091	0.762	11.592	3.248	0.408
0.25	196.710	0.091	0.740	10.539	3.290	0.487
0.30	199.745	0.091	0.719	9.561	3.348	0.561
0.35	203.400	0.091	0.698	8.664	3.424	0.627
0.40	207.593	0.091	0.679	7.853	3.518	0.687
0.45	212.241	0.090	0.662	7.126	3.630	0.741
0.50	217.268	0.090	0.647	6.481	3.759	0.787
0.55	222.613	0.089	0.635	5.915	3.906	0.828
0.60	228.205	0.088	0.623	5.426	4.069	0.862
0.65	234.018	0.087	0.614	5.012	4.249	0.890
0.70	240.031	0.086	0.605	4.670	4.443	0.912
0.75	246.227	0.085	0.598	4.395	4.652	0.929
0.80	252.632	0.085	0.591	4.182	4.875	0.941
0.85	259.318	0.085	0.586	4.023	5.109	0.949
0.90	266.361	0.084	0.582	3.913	5.353	0.953
0.95	273.853	0.084	0.581	3.846	5.607	0.953
1.00	281.886	0.084	0.583	3.823	5.870	0.950

Note: Values in bold represent the optimal point obtained through the fuzzy DM.

multivariate confidence intervals for confirmation runs. With a power of 80%, the hypothesis test can detect the difference of at least one pass in the turning machine, as shown in Fig. 12, and with a pre-test value of 0.533 as standard deviation, the sample size is found to be 5. A series of five experiments run under optimal experimental conditions with the fuzzy NBI-MMSE approach yielded $V_c = 273.853$ [m/min], $f = 0.084$ [mm/rev], and $d = 0.581$ [mm].

Surface roughness was measured at four points of the workpiece, at 90° intervals at diameters of 30 and 50 mm, with flank tool wear values of ~ 0.0 and ~ 0.3 mm (Fig. 13). The mean of these measurements are reported on Table 10. Fig. 14 illustrates the snapshot from confirmation run #5 in the worst case: 50 mm of diameter and a flank tool wear of 0.3 mm.

Also, it is possible to infer from Fig. 15 that the variation of the roughness in the piece (CP, CE, and CA) has become minimal. That is,

the optimum setup found for the machine provided similar roughness measurements throughout the piece even if the piece is long. Therefore, it is concluded that the roughness values measured under the 12 noise conditions are smaller than those of the original experiment (run #13). It can be seen that the mean values for R_a obtained with the confirmation runs are quite close to the predicted ones, which demonstrates that the setup is robust to the presence of noise.

At a confidence level of 95%, the bidimensional confidence ellipses for the dual-response surface models (A–H) were constructed to verify whether the Pareto solution belongs to the ellipses' interval. Through Fig. 16, it is noticed that the bidimensional confirmation run vector falls within the confidence ellipse only in the representation of Model B, thus affirming which model of estimators achieves the best RPD solution. Tables 11 and 12 detail the confirmation runs modeled by location and scale estimators and the upper and lower bounds for 95% multivariate

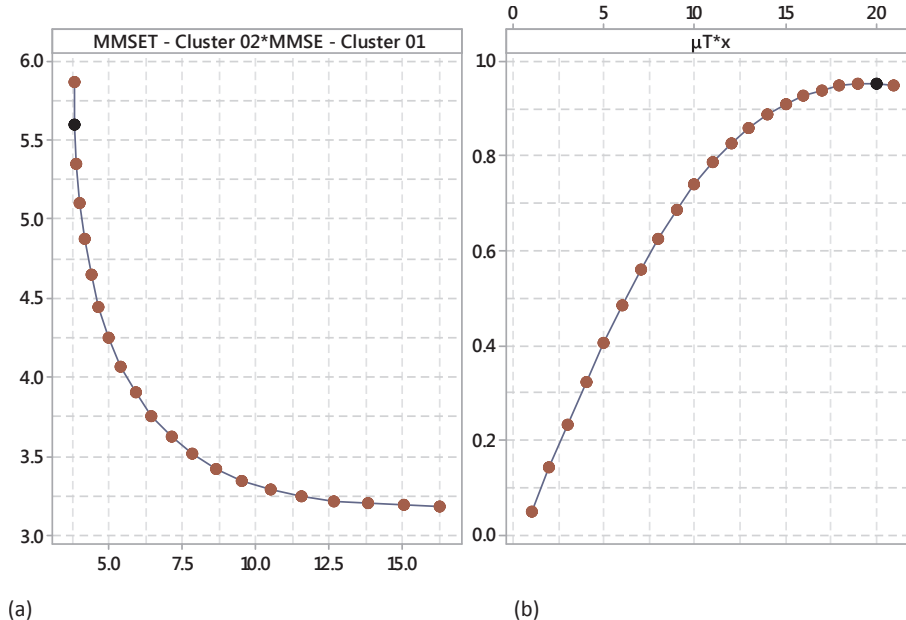


Fig. 10. (a) Pareto frontier obtained by the NBI method and (b) total membership.

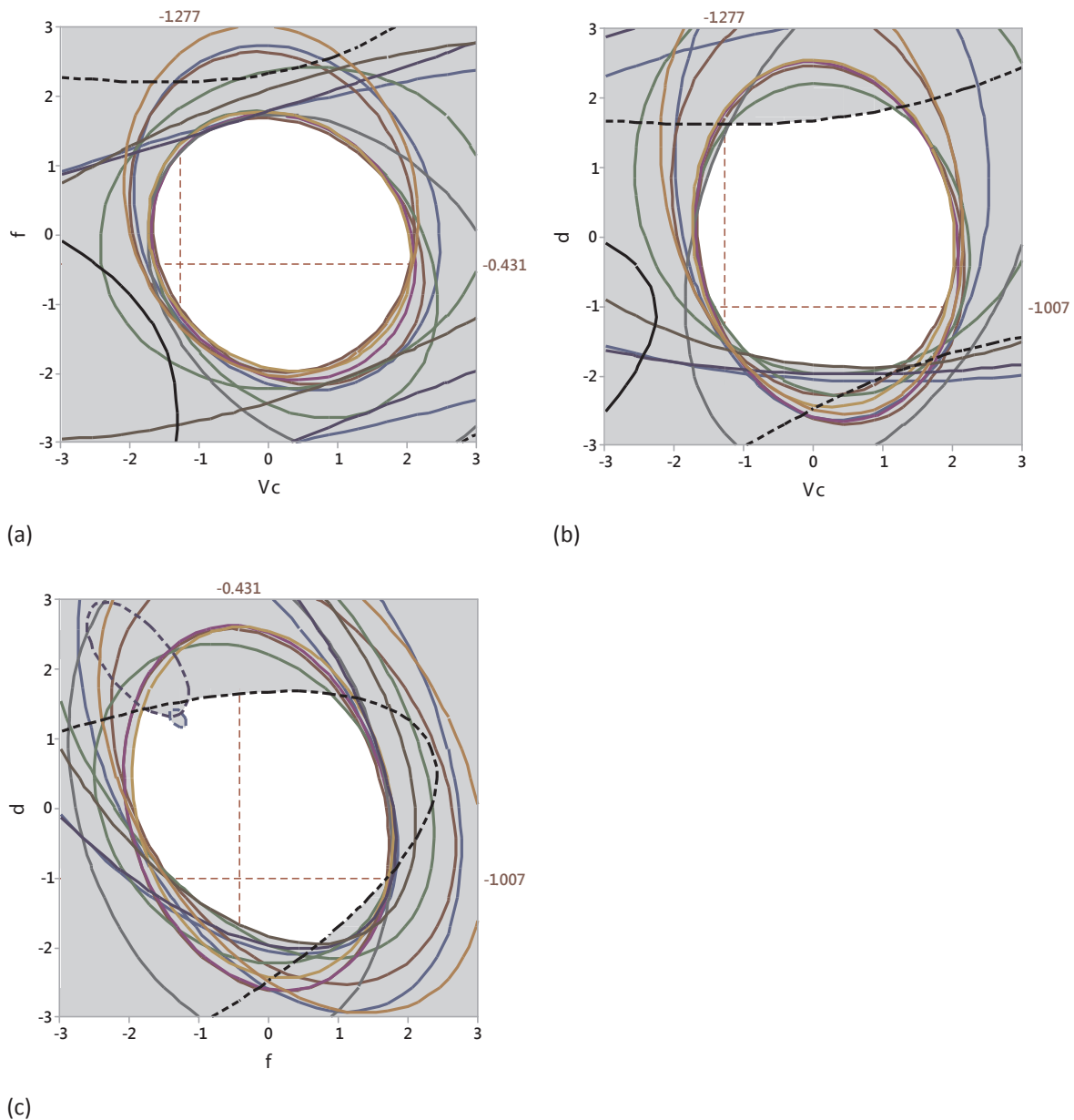


Fig. 11. Overlaid contour graphics of original responses.

confidence intervals following the expression given by Eq. (13). Also shown are the sum of squares that represents the squared differences of each observation from the centroid, thus supporting the choice of Model B because it has the lower value of distance.

As mentioned in Section 2, the breakdown point is a measure of robustness of an estimator and, roughly, is the smallest fraction of atypical points that can take the estimator beyond any limit. Both the median and the MAD have a breakdown point of 50%, which is the highest possible, thus reinforcing their robustness for modeling.

Because the results are compatible with the expected values and

turning theory, the fuzzy NBI-MMSE method may be considered suitable for improving the machining process even in the presence of noise interference. In conclusion, modeling responses by using robust estimators allowed an adequate representation of the surface roughness.

5.1. Machining parameters comparison

Since the best machining parameters were defined through the proposed algorithm of optimization (NBI-MMSE) and thus confirmed by confirmation runs, another comparison on the machined surface under

Table 8
Optimized values of the R_a modeled data.

Limit	Location and scale response surfaces												
	\bar{x}	s	\bar{x}	MAD	\bar{x}_{H2}	s_{H2}	HL_n	S_n	Q_n	\bar{x}_τ	s_τ	\bar{x}_{MLE}	S_{MLE}
Lower	1.444	0.298	1.095	0.167	1.322	0.296	1.279	0.231	0.272	1.068	0.277	1.491	0.246
Upper	2.412	1.926	2.203	1.273	2.103	1.108	1.900	1.271	1.148	2.001	1.070	2.899	1.383

Table 9
Optimized values of the R_a modeled data.

w	Location and scale estimators												
	\bar{x}	\tilde{x}	\tilde{x}_{H2}	HL_n	\tilde{x}_τ	\tilde{x}_{MLE}	s	MAD	s_{H2}	S_n	Q_n	s_τ	S_{MLE}
0.00	1.721	1.171	1.337	1.298	1.126	2.273	1.372	0.172	0.429	0.238	0.302	0.235	1.022
0.05	1.705	1.170	1.337	1.299	1.123	2.230	1.319	0.179	0.436	0.241	0.296	0.240	0.990
0.10	1.690	1.172	1.340	1.302	1.122	2.185	1.265	0.191	0.448	0.247	0.295	0.248	0.956
0.15	1.675	1.176	1.346	1.307	1.124	2.138	1.210	0.205	0.463	0.259	0.297	0.260	0.922
0.20	1.659	1.180	1.353	1.314	1.127	2.089	1.155	0.223	0.481	0.274	0.302	0.274	0.887
0.25	1.643	1.185	1.361	1.322	1.131	2.039	1.101	0.243	0.501	0.294	0.310	0.291	0.852
0.30	1.627	1.189	1.369	1.330	1.135	1.989	1.048	0.264	0.523	0.317	0.321	0.310	0.817
0.35	1.609	1.192	1.377	1.339	1.139	1.939	0.997	0.286	0.546	0.341	0.333	0.331	0.782
0.40	1.591	1.194	1.385	1.347	1.142	1.891	0.948	0.308	0.569	0.368	0.348	0.352	0.749
0.45	1.573	1.194	1.392	1.356	1.144	1.843	0.901	0.330	0.591	0.395	0.364	0.374	0.716
0.50	1.554	1.192	1.399	1.364	1.146	1.797	0.855	0.352	0.613	0.422	0.381	0.396	0.685
0.55	1.536	1.191	1.405	1.373	1.149	1.752	0.811	0.373	0.634	0.450	0.401	0.418	0.655
0.60	1.519	1.191	1.413	1.382	1.153	1.709	0.768	0.394	0.654	0.477	0.422	0.441	0.626
0.65	1.503	1.192	1.421	1.393	1.159	1.668	0.726	0.416	0.673	0.506	0.445	0.466	0.598
0.70	1.489	1.196	1.431	1.406	1.167	1.630	0.686	0.439	0.692	0.535	0.469	0.491	0.572
0.75	1.478	1.202	1.443	1.421	1.177	1.596	0.648	0.464	0.711	0.566	0.495	0.518	0.548
0.80	1.470	1.211	1.456	1.437	1.190	1.565	0.612	0.490	0.730	0.597	0.522	0.547	0.527
0.85	1.465	1.221	1.471	1.455	1.204	1.539	0.580	0.517	0.748	0.629	0.551	0.576	0.509
0.90	1.462	1.233	1.486	1.473	1.220	1.518	0.553	0.543	0.765	0.661	0.580	0.605	0.495
0.95	1.461	1.244	1.501	1.491	1.235	1.502	0.533	0.569	0.782	0.692	0.612	0.635	0.487
1.00	1.464	1.254	1.515	1.508	1.249	1.494	0.521	0.592	0.799	0.720	0.645	0.663	0.486

Note: Values in bold represent the optimal point obtained through the fuzzy DM.

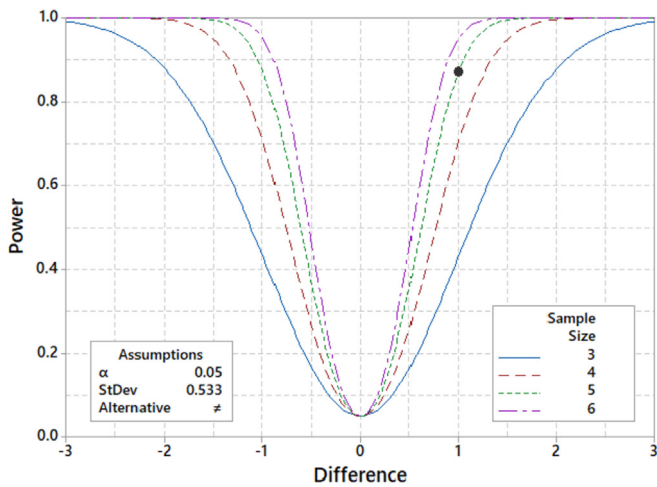


Fig. 12. Sample size calculation for confirmation runs (power = 80%; $\alpha = 5\%$; $\sigma = 0.533$ min).

Table 10

Confirmation run means for fuzzy NBI-MMSE method at $w = 0.95$ for AISI 12L14 turning.

n	ϕ 30 mm – VB = 0.0	ϕ 50 mm – VB = 0.0	ϕ 30 mm – VB = 0.3	ϕ 50 mm – VB = 0.3
1	1.184	0.858	1.378	1.683
2	0.997	0.905	1.450	1.677
3	0.808	0.764	1.654	1.783
4	1.178	0.851	1.585	1.777
5	1.005	1.010	1.494	1.982

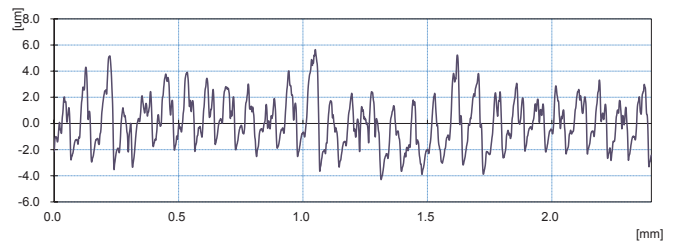


Fig. 14. Profile measure of worst condition (higher R_a) for diameter = 50 mm and VB = 0.3 mm.

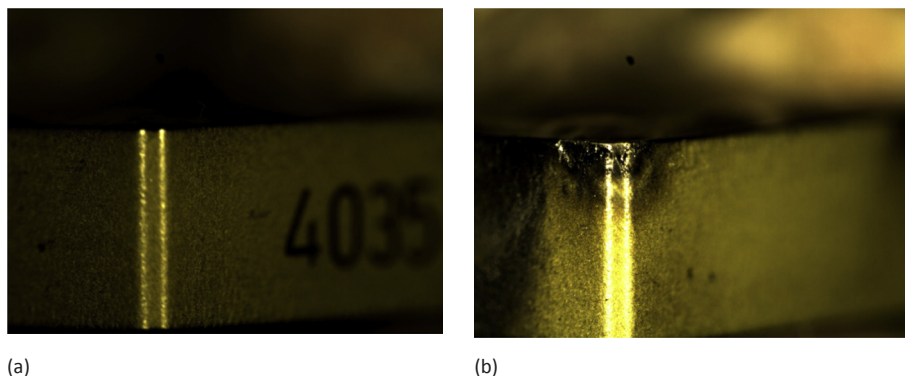


Fig. 13. AISI 12L14 turning microscope for VB of (a) ~ 0.0 mm and (b) ~ 0.3 mm.

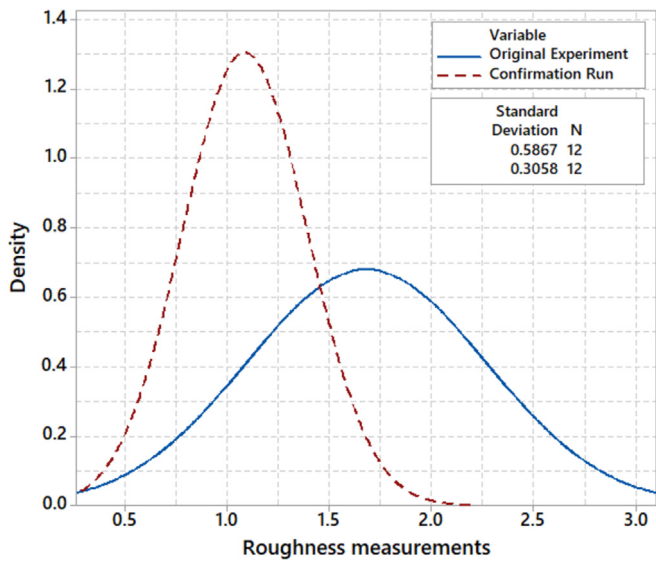


Fig. 15. Roughness standard deviations of original experiment versus confirmation run.

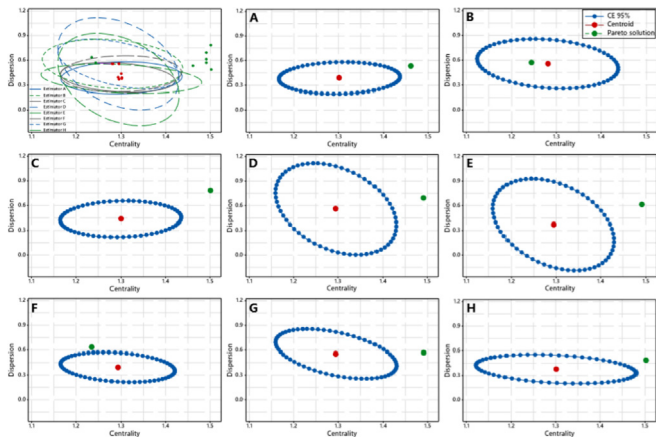


Fig. 16. 95% confidence ellipses of model estimators.

Table 11 Confirmation runs modeled by location and scale estimators for Models A–D.

Run	Location and scale response surfaces							
	A		B		C		D	
	\bar{x}	s	\bar{x}	MAD	\bar{x}_{H2}	s_{H2}	HL_n	S_n
1	1.276	0.346	1.281	0.370	1.276	0.392	1.276	0.371
2	1.257	0.367	1.224	0.404	1.257	0.417	1.257	0.516
3	1.252	0.541	1.231	0.660	1.252	0.613	1.252	0.962
4	1.348	0.415	1.382	0.444	1.348	0.470	1.348	0.463
5	1.373	0.466	1.252	0.362	1.373	0.529	1.373	0.554
Centroid	1.301	0.388	1.281	0.555	1.300	0.437	1.295	0.561
CI UB ^a	1.437	0.581	1.438	0.855	1.435	0.655	1.430	1.118
Pareto	1.461	0.533	1.244	0.569	1.501	0.782	1.491	0.692
CI LB ^b	1.166	0.195	1.124	0.255	1.164	0.218	1.159	0.003
SST	1.956	–	1.786	–	1.985	–	1.974	–

Note: The values in bold represent the best RPD solution.

^a CI UB: Multivariate upper bound for confidence interval.

^b CI LB: Multivariate lower bound for confidence interval.

different parameters was done. This approach was performed in order to compare the machined surface picture under the best condition with pictures from other turning test.

Using the same power and sample size capabilities detailed on Step

Table 12 Confirmation runs modeled by location and scale estimators for Models E–H.

Run	Location and scale response surfaces							
	E		F		G		H	
	HL_n	Q_n	\bar{x}_r	s_r	HL_n	MAD	\bar{x}_{MLE}	S_{MLE}
1	1.276	0.372	1.279	0.312	1.276	0.370	1.276	0.300
2	1.257	0.516	1.241	0.331	1.257	0.404	1.279	0.287
3	1.252	0.963	1.246	0.487	1.252	0.660	1.252	0.469
4	1.348	0.463	1.367	0.374	1.348	0.444	1.336	0.339
5	1.373	0.555	1.255	0.438	1.373	0.362	1.435	0.331
Centroid	1.295	0.370	1.293	0.393	1.295	0.555	1.301	0.378
CI UB ^a	1.430	0.928	1.421	0.573	1.430	0.855	1.481	0.555
Pareto	1.491	0.612	1.235	0.635	1.491	0.569	1.502	0.487
CI LB ^b	1.159	–0.188	1.165	0.214	1.159	0.255	1.121	0.201
SST	1.974	–	1.788	–	1.974	–	1.987	–

Note.

^a CI UB: Multivariate upper bound for confidence interval.

^b CI LB: Multivariate lower bound for confidence interval.

8, Fig. 12 illustrates the best possible number of sample size which was 5. Therefore, a series of five experiments run under center point experimental condition yielded $V_c = 280.00$ [m/min], $f = 0.10$ [mm/rev], and $d = 0.95$ [mm]. These machining parameters input were chosen since the center point runs provide a measure of process stability and inherent variability and also check the model curvature.

Surface roughness was measured at four points of the workpiece, at 90° intervals at diameters of 30 and 50 mm, with flank tool wear values of ~0.0 and ~0.3 mm (Fig. 13). The mean of these measurements are reported on Table 13.

It is possible to infer from Fig. 17 that the variation of the roughness in the center point machining parameters - $V_c = 280.00$ [m/min], $f = 0.10$ [mm/rev], and $d = 0.95$ [mm] – has not become minimal. Therefore, it is concluded that the roughness values measured under the 12 noise conditions are equal than those of the original experiment (run #13) and are greater than the optimum setup defined by the NBI-MMSE algorithm of optimization. It can be seen that the mean values for R_a obtained with the center point runs are higher to the predicted ones. This analysis reinforces that the setup defined by NBI-MMSE is robust to the presence of noise.

Through Fig. 18 it is noted that the surface finish chart fancy machining of confirmation run has shallower grooves in relation to the experiment performed with the center point parameters. To determine these pictures a Digital Microscope U1600X was used where the golden color scale indicates the live center of each piece. Figs. 19 and 20 illustrates the roughness snapshot from optimal setup and from center point setup (setup of comparison); thus reaffirming that the surface finish provided by the optimal setup (NBI-MMSE method) is better.

A scanning electron microscopy (SEM) was applied for surface morphology examination. The workpieces' surfaces were analyzed in the SEM with the objective of verifying the roughness on the machined material. This experiment was developed in the Structural Characterization Laboratory (ECL) of Federal University of Itajubá (UNIFEI). Figs. 21 and 22 show the analysis of the machining peaks for a feed rate of $f = 0.084$ mm/rev and of $f = 0.100$ mm/rev, respectively.

Table 13 Center point experimental run for AISI 12L14 turning.

n	ϕ 30 mm – VB = 0.0	ϕ 50 mm – VB = 0.0	ϕ 30 mm – VB = 0.3	ϕ 50 mm – VB = 0.3
1	1.213	1.168	1.798	2.388
2	1.253	1.178	1.900	2.095
3	1.183	1.183	1.670	2.123
4	1.188	1.188	1.730	2.600
5	1.213	1.193	1.893	2.895

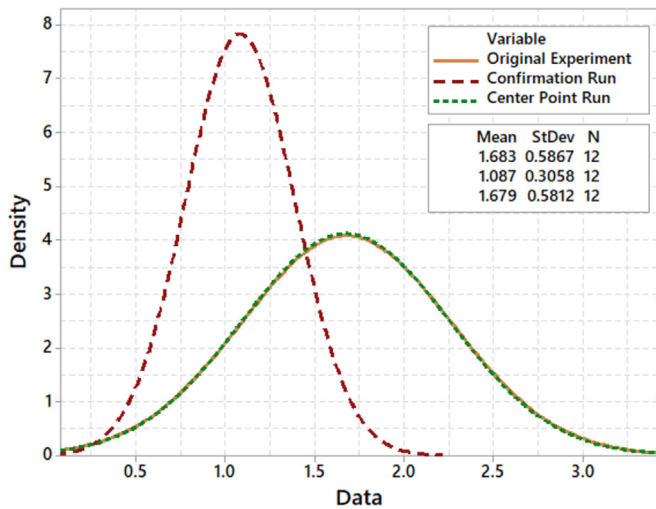


Fig. 17. Roughness standard deviations of machining parameters run.

The roughness value for the workpiece machined with $f = 0.100$ mm/rev were larger than the one machined with $f = 0.084$ mm/rev indicating the optimal setup through the NBI-MMSE method.

In parallel, the Energy Dispersive X-ray Spectrometry (EDS) was done which makes use of the X-ray spectrum emitted by a solid sample bombarded with a focused beam of electrons to obtain a localized chemical analysis. All elements from atomic number 4 (Be) to 92 (U) can be detected in principle, though not all instruments are equipped for 'light' elements as the carbon and nitrogen existing in the AISI 12L14 steel according to the chemical elements detailed in Table 14 and also in Figs. 23 and 24.

6. Comparison with genetic algorithm

The extension of NBI-MMSE approach was evaluated in order to extent their methodology and determines how the results improve against the modern genetic intelligence algorithms. Therefore, the *gamultiobj* function which find Pareto front of multiple fitness functions

using genetic algorithm was implemented.

6.1. MMSE functions optimization through algorithm genetic

Considering Eq. (32) in which was detailed the objective functions to be optimized in terms of MMSE, the multi-objective genetic algorithm was running with the experimental restriction $\bar{g}_2(x) = x^T x \leq \rho^2$ and with lower and upper bounds for each input parameter according to the description in Appendix A. This optimization was performed in MATLAB® R2015a.

Fig. 25 shows the optimal points found by the *gamultiobj* function as detailed in Table 15. In sequence, these optimal values were replaced in Eq. (32) in order to find the functions in terms of MMSE. Considering MMSE values, the Pareto frontier obtained by the GRG algorithm (Fig. 10) was plotted together as shown in Fig. 26. It is possible to notice that the frontiers are practically overlapping and thus reaffirming that the proposed method is capable of generating convex frontiers independent of the algorithm.

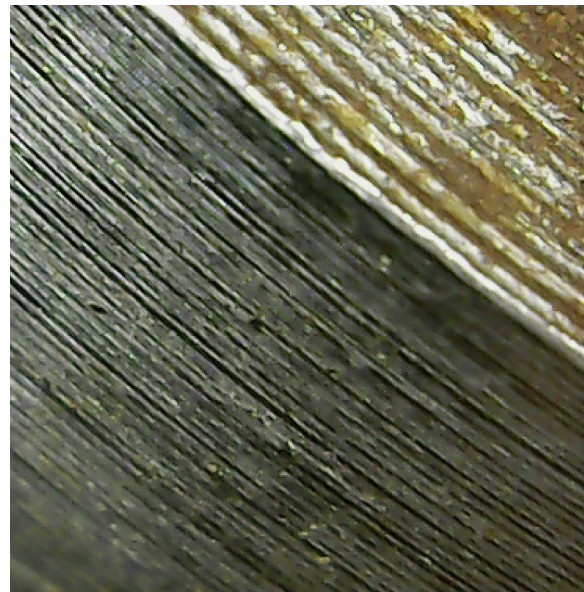
6.2. Optimization of original functions modeled by robust estimators

In order to verify the robustness of the research methodology proposed through 8 steps detailed in Fig. 5, the *gamultiobj* function was applied in the 13 original responses obtained by the roughness (R_a) modeling as shown in Table 5. The objective of this optimization is to show the importance of the 8 steps proposed in the modeling stage that affect the problem optimal setups according to the description in Appendix B.

After the optimization performed by the MATLAB®, Table 16 shows the optimal points found by the *gamultiobj* function. In sequence, these optimal values were replaced in Eq. (32) in order to find the functions in terms of MMSE. Considering the MMSE values in Table 16, the Pareto frontier obtained by the GRG algorithm (Fig. 10) was plotted together as shown in Fig. 27. It is possible to notice that the frontier defined by 8 steps proposed herein (NBI-MMSE algorithm of optimization) has dominance in relation to the optimal points obtained by the *gamultiobj* function.



(a) Optimal setup:
 $V_c = 273.853$ [m/min], $f = 0.084$ [mm/rev], $d = 0.581$ [mm]



(b) Setup of comparison:
 $V_c = 280.00$ [m/min], $f = 0.10$ [mm/rev], $d = 0.95$ [mm]

Fig. 18. Surface finish chart fancy machining of (a) confirmation run and (b) center point run.

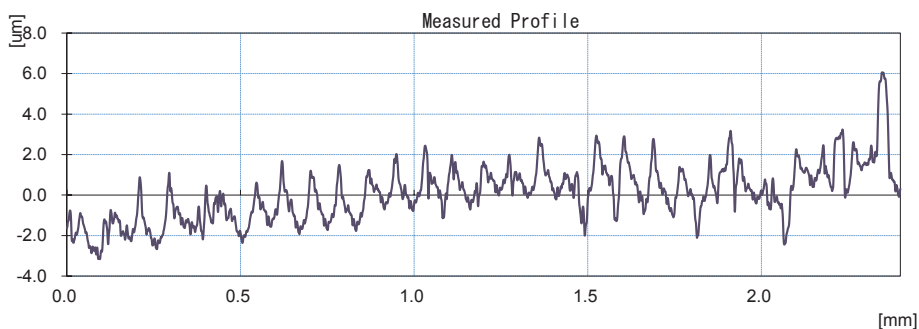


Fig. 19. Profile measure of optimal setup.

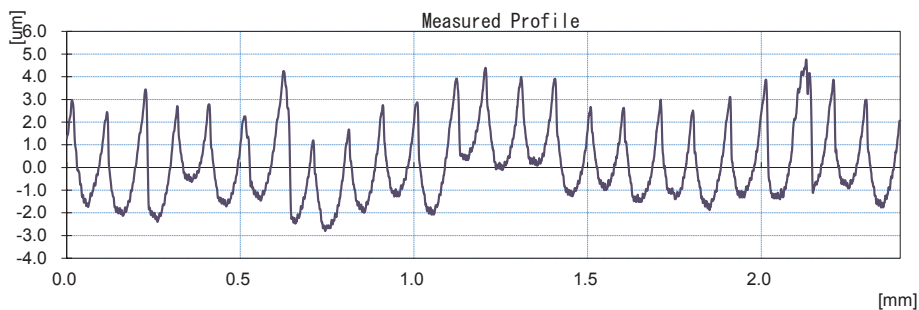


Fig. 20. Profile measure of setup of comparison (center point).

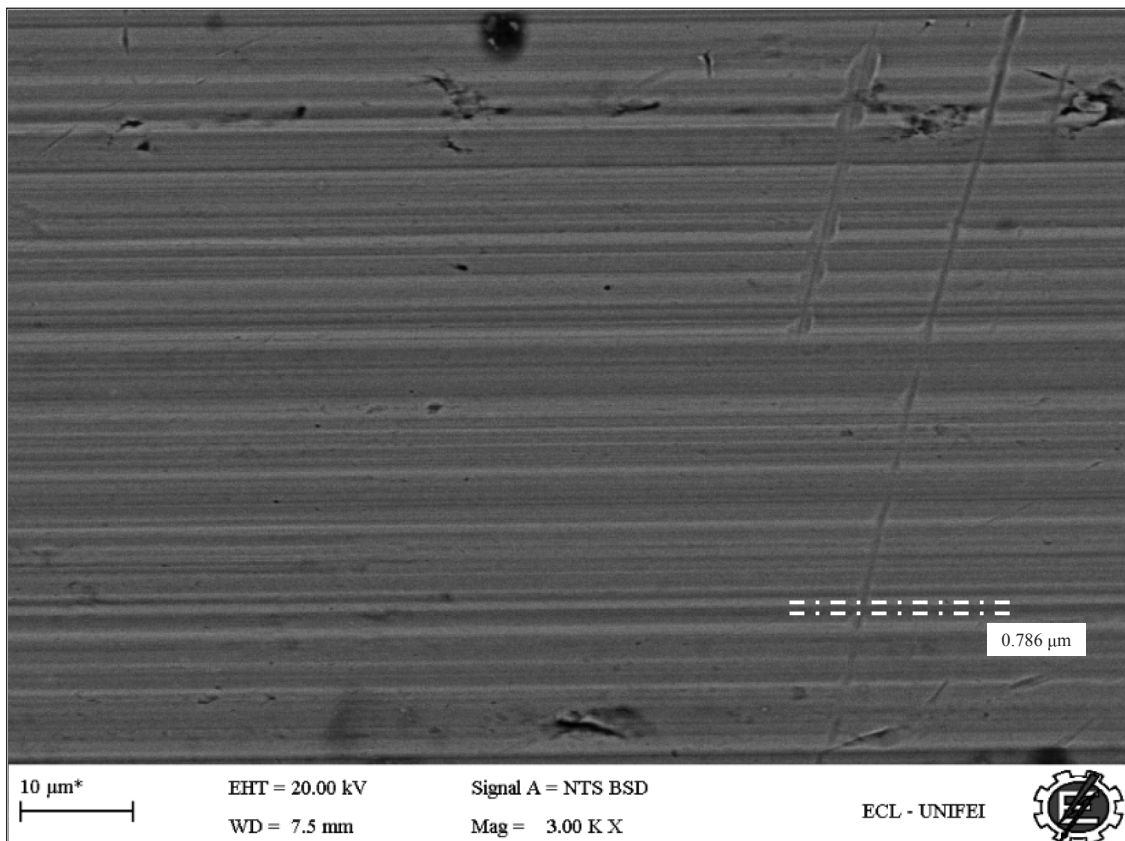


Fig. 21. Distance between peaks for the optimal setup ($f=0.084$ mm/rev).

7. Conclusion

In this paper, the use of robust estimators to model the surface roughness of an AISI 12L14 steel turning process was presented. The main contribution of this paper consists of the application and

contextualization of PCA to determine the process parameter setups that are capable of reducing the surface roughness dispersion along with multivariate optimization techniques. Accordingly, a novel algorithm considering objective functions in terms of the MMSE values, which were optimized through the NBI method, was proposed to obtain

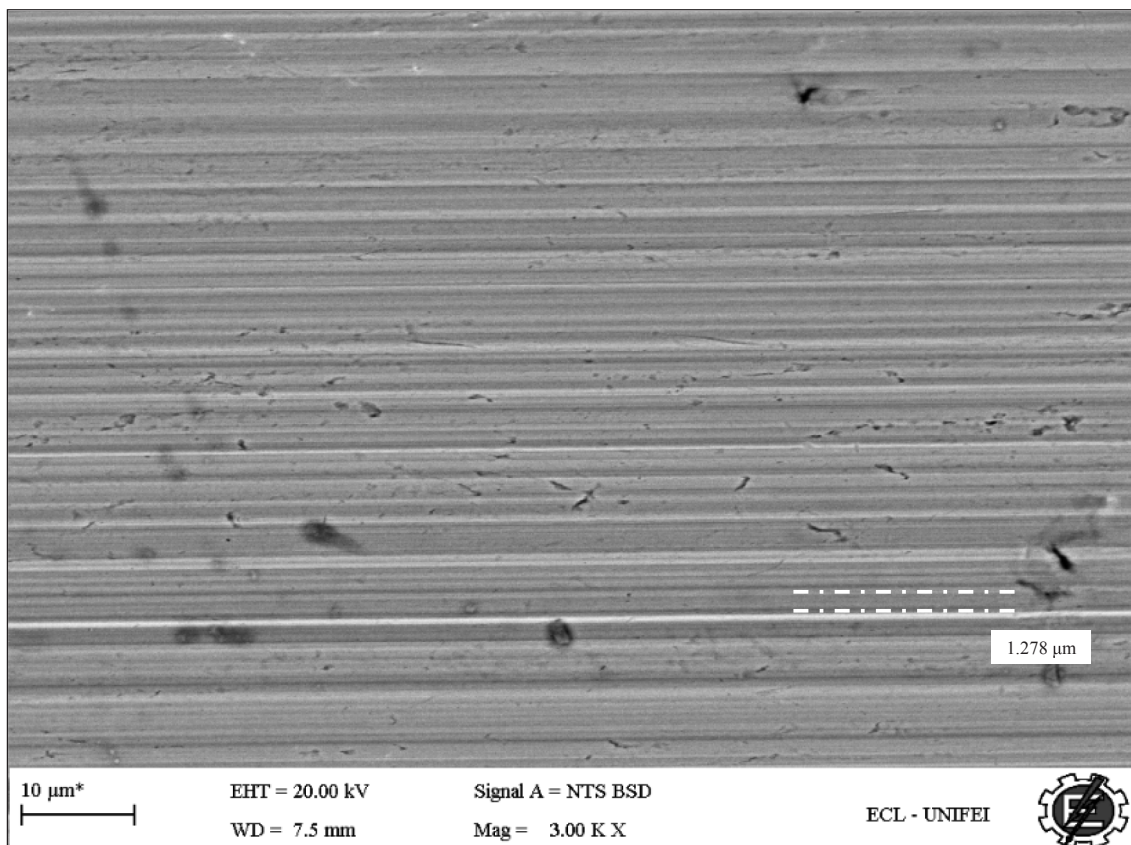
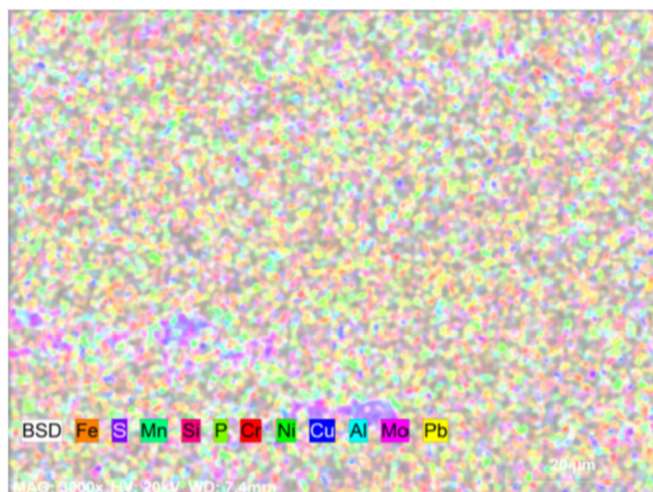


Fig. 22. Distance between peaks for the setup of comparison ($f=0.100$ mm/rev).

Table 14

Chemical composition of AISI 12L14.

%C	%Si	%Mn	%P	%S	%Cr	%Ni	%Cu	%Al	%Mo	%Pb	%N
0.090	0.030	1.240	0.046	0.273	0.150	0.080	0.260	0.001	0.020	0.280	0.0079



Confirmacao
Date:12/18/2018 6:45:00 PM
Image size:1024 x 768
Mag:3000x
HV:20.0kV

Fig. 23. Chemical elements in AISI 12L14 steel.

a feasible solution represented by a Pareto frontier. Consequently, another contribution is defining the Pareto optimal point by using fuzzy DM reinforced by the 95% confidence ellipses of the estimators' models for confirmation runs.

Therefore, taking into account all the discussions presented in the proposed steps, we can conclude the following:

- Noise conditions intrinsic in the turning process provide the non-normality of the data (not stationary), thus providing variation with extreme points. This scenario emphasizes the use of robust estimators to model the data.
- Optimization of the surface roughness centrality and dispersion models was done by using the NBI method, thus assuring convex frontiers and equispaced optimal points.
- The MMSE minimizes all the original responses simultaneously with their respective targets expressed in terms of principal components to obtain a solution that considers the best of all estimators.
- With the fuzzy DM algorithm, it is possible to define the best process input parameters as $V_c = 273.853$ [m/min], $f = 0.084$ [mm/rev], and $d = 0.583$ [mm].
- Experimental confirmation runs were able to obtain the optimum output values defined by the algorithm.
- The 95% confidence ellipses considering the data obtained through the confirmation runs define which pair of estimators performs best models the experimental data under noise conditions. It was determined that Model B (which comprises the nonparametric

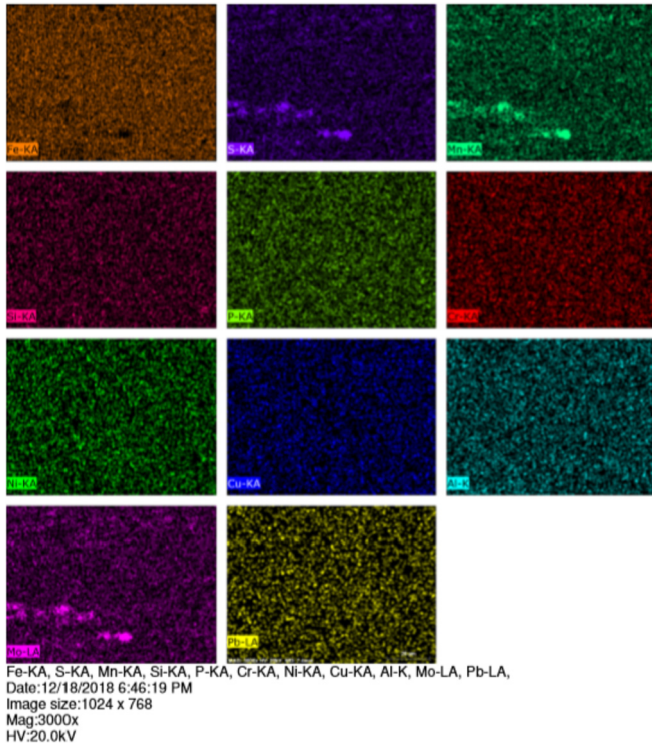


Fig. 24. Chemical elements in AISI 12L14 steel in isolation.

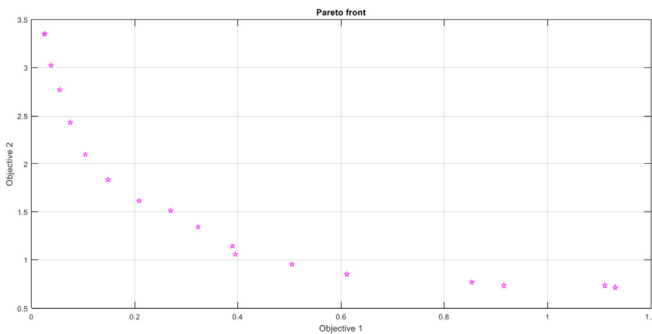


Fig. 25. Pareto front of $\tilde{f}_1(x)$ and $\tilde{f}_2(x)$ scalarized.

Table 15
Optimum values obtained by MMSE functions optimization.

	$\tilde{f}_1(x)$	$\tilde{f}_2(x)$	$x_1 (V_c)$	$x_2 (f)$	$x_3 (d)$	$MMSE_1^1$	$MMSE_2^T$
1	0.025	3.348	-0.436	-0.699	-1.467	4.137	4.934
2	0.105	2.099	-0.785	-0.686	-1.318	5.136	4.200
3	0.915	0.736	-1.362	-0.866	-0.472	15.255	3.213
4	0.269	1.513	-1.009	-0.721	-1.095	7.185	3.807
5	0.149	1.837	-0.848	-0.801	-1.209	5.687	4.029
6	0.075	2.434	-0.685	-0.700	-1.365	4.762	4.409
7	1.131	0.718	-1.394	-0.888	-0.309	17.961	3.198
8	0.038	3.022	-0.522	-0.701	-1.436	4.303	4.754
9	0.611	0.850	-1.300	-0.775	-0.735	11.455	3.307
10	0.025	3.348	-0.436	-0.699	-1.467	4.137	4.934
11	0.208	1.617	-0.946	-0.755	-1.152	6.420	3.880
12	0.854	0.762	-1.336	-0.875	-0.519	14.496	3.234
13	0.505	0.951	-1.236	-0.779	-0.829	10.138	3.388
14	0.395	1.054	-1.196	-0.687	-0.958	8.763	3.468
15	0.055	2.765	-0.597	-0.699	-1.403	4.513	4.606
16	0.323	1.344	-1.071	-0.732	-1.030	7.864	3.686
17	0.390	1.144	-1.159	-0.703	-0.965	8.699	3.538
18	1.111	0.734	-1.370	-0.905	-0.324	17.711	3.211

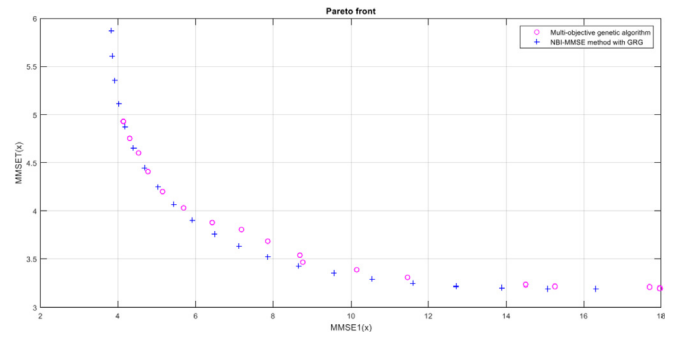


Fig. 26. Comparative Pareto frontier between genetic algorithm and NBI-MMSE algorithm.

Table 16
Optimum values obtained by the optimization of roughness modeled responses.

	$x_1 (V_c)$	$x_2 (f)$	$x_3 (d)$	$MMSE_1^1$	$MMSE_2^T$
1	-1.196	-0.961	-0.671	11.769	3.375
2	-1.450	-0.814	-0.247	19.076	3.212
3	-1.188	-0.921	-0.742	10.863	3.405
4	-1.458	-0.682	-0.472	15.530	3.197
5	-1.095	-0.908	-0.894	8.784	3.551
6	-0.559	1.505	0.504	4.542	11.309
7	-0.357	-0.959	-1.299	4.407	5.119
8	-0.320	1.566	0.514	4.629	11.513
9	-1.450	-0.814	0.253	27.452	3.838
10	-0.816	-0.937	-1.097	6.292	4.080
11	-1.411	-0.877	0.253	27.695	3.816
12	0.442	-1.007	-1.256	4.260	6.732
13	-0.011	0.891	-1.222	8.490	10.495
14	-0.148	1.255	0.590	9.432	13.903
15	0.411	-0.985	-1.291	4.141	6.639
16	-0.320	1.566	0.514	4.629	11.513
17	-0.410	1.192	-0.291	9.734	12.901
18	-1.154	0.591	-0.578	10.902	7.095

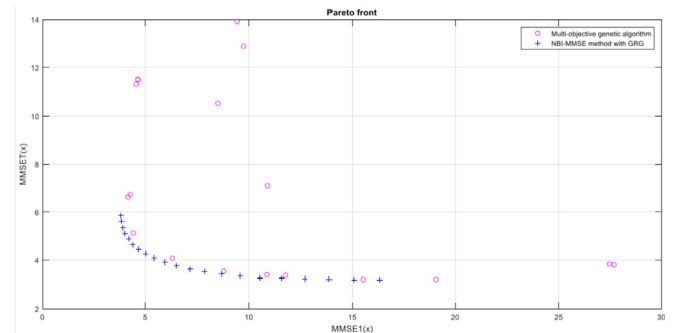


Fig. 27. Comparative Pareto frontier between NBI-MMSE algorithm and roughness responses optimized by genetic algorithm.

estimators as the median and the MAD) is better. Consequently, the centrality value of R_a is 1.281 with a minimal value of dispersion of 0.555.

- In situations where the experimental responses are influenced by the presence of noise, the modeling can be performed with robust estimators that cancel or minimize this influence. However, the use of parameter estimators is not discarded.
- In order to verify the robustness of the optimal setup defined by the NBI-MMSE proposed method, it was compared with the center point setup. Through roughness pictures it is possible to reaffirming that the surface finish is better than the others;
- Optimal points were also defined by the multi-objective genetic algorithm (MOGA) which proved the efficiency of the modeling proposed stages.

The proposed method can identify the optimal solution within the limits specified for the machining process to obtain the most efficient production. Another relevant factor is that the method becomes more advantageous as the number of functions increases because it enables a dimensionality reduction that leads to computational advantages.

Finally, the decision-making process in the manufacturing environment is increasingly difficult owing to the rapid changes in design and demand for quality products. Therefore, industries need to maintain machined surface quality and can consequently reduce inspection costs and increase productivity. The proposed method can be easily extended to other machining processes so that environmental concerns can be well addressed together with the objectives of productivity and quality.

Acknowledgements

The authors thank to the Brazilian agencies of CAPES and CNPq that provided financial support (Processes n° 303586/2015-0 and 153299/2018-5). We also thank the Prof. PhD. Geovani Rodrigues and the technician in metallurgy Jonas Medes from the University Federal of Itajubá (UNIFEI), Brazil, who allowed the SEM and EDS experiments.

Appendix A. Supplementary data

Supplementary data related to this article can be found at <https://doi.org/10.1016/j.precisioneng.2019.01.001>.

References

- [1] Montgomery DC. Design and analysis of experiments. sixth ed. New York: John Wiley; 2005.
- [2] Ardakani MK, Wulff SS. An overview of optimization formulations for multiresponse surface problems. *Qual Reliab Eng Int* 2013;29(1):3–16.
- [3] Alaeddini A, Yang K, Murat A. ASRSM: a sequential experimentation design for response surface optimization. *Qual Reliab Eng Int* 2013;29–2:241–58.
- [4] Robinson TJ, Borror CM, Myers RH. Robust parameter design: a review. *Qual Reliab Eng Int* 2004;20–1:81–101.
- [5] Myers RH, Carter WH. Response surface techniques for dual response systems. *Technometrics* 1973;15–2:301–17.
- [6] Vining GG, Myers RH. Combining Taguchi and response surface philosophies: a dual response approach. *J Qual Technol* 1990;22–1:38–45.
- [7] Boylan GL, Cho BR. Comparative studies on the high-variability embedded robust parameter design from the perspective estimators. *Comput Ind Eng* 2013;64:442–52.
- [8] Liu Z, Song R, Zeng D, Zhang J. Principal components adjusted variable screening. *Comput Stat Data Anal* 2017;110:134–44.
- [9] Costa DM, Brito TG, Paiva AP, Leme RC, Balestrassi PP. A normal boundary intersection with multivariate mean square error approach for dry end milling process optimization of the AISI 1045 steel. *J Clean Prod* 2016;135:1658–72.
- [10] Das I, Dennis JE. Normal-Boundary Intersection: a new method for generating the Pareto surface in nonlinear multicriteria optimization problems. *Soc Ind Appl Math* 1998;8–3:631–57.
- [11] Peruchi RS, Balestrassi PP, Paiva AP, Ferreira JR, Carmelossi MS. A new multivariate gage R&R method for correlated characteristics. *Int J Prod Econ* 2013;144:301–15.
- [12] Fountas NA, Benhadj-Djilali R, Stergiou CI, Vaxevanidis NM. An integrated framework for optimizing sculptured surface CNC tool paths based on direct software object evaluation and viral intelligence. *J Intell Manuf* 2017;1–19.
- [13] Fountas NA, Seretis GV, Manolakos DE, Provatidis CG, Vaxevanidis NM. Multi-objective statistical analysis and optimisation in turning of aluminium matrix particulate composite using genetic algorithm. *Int J Mach Mach Mater* 2018;20(3):236–51.
- [14] Newman ST, Nassehi A, Imani-Asrai R, Dhokia V. Energy efficient process planning for CNC machining. *CIRP J Manuf Sci Technol* 2012;5(2):127–36.
- [15] Agostinelli C, Locatelli I, Marazzi A, Yohai VJ. Robust estimators of accelerated failure time regression with generalized log-gamma errors. *Comput Stat Data Anal* 2017;107:92–106.
- [16] Lee SB, Park C, Cho BR. Development of a highly efficient and resistant robust design. *Int J Prod Res* 2007;45(1):157–67.
- [17] Yohai VJ, Zamar RH. High breakdown-point estimates of regression by means of the minimization of an efficient scale. *J Am Stat Assoc* 1988;83(402):406–13.
- [18] Serfling R. Asymptotic relative efficiency in estimation. *International encyclopedia of statistical sciences*; 2011. p. 68–72.
- [19] Maronna RA, Martin DR, Yohai VJ. Robust statistics: theory and methods. New York: John Wiley; 2006.
- [20] Rousseeuw PJ, Croux C. Alternatives to the median absolute deviation. *J Am Stat Assoc* 1993;88–424:1273–83.
- [21] Leys C, Ley C, Klein O, Bernard P, Licata L. Detecting outliers: do not use standard deviation around the mean, use absolute deviation around the median. *J Exp Soc Psychol* 2013;49–4:764–6.
- [22] Hampel FR. The influence curve and its role in robust estimation. *J Am Stat Assoc* 1974;69–346:383–93.
- [23] Rousseeuw PJ, Croux C. Explicit scale estimators with high breakdown point. *Stat Anal Relat Meth* 1992:77–92.
- [24] Hodges JL, Lehmann EL. Estimates of location based on rank tests. *Ann Math Stat* 1963;34–2:598–611.
- [25] Serfling R. Asymptotic relative efficiency in estimation. *International encyclopedia of statistical sciences*; 2011. p. 68–72.
- [26] Huber PJ. Robust estimation of a location parameter. *Ann Math Stat* 1964;35–1:73–101.
- [27] Huber PJ. Robust statistics. Hoboken, NJ, USA: John Wiley & Sons, Inc.; 1981.
- [28] Maronna RA, Zamar RH. Robust estimates of location and dispersion for high-dimensional datasets. *Technometrics* 2002;44–4:307–17.
- [29] Elias SR. Maximum likelihood estimation: logic and practice. 96th ed. USA: Sage Publications; 1993.
- [30] O'Hagan A, Leonard T. Bayes estimation subject to uncertainty about parameter constraints. *Biometrika* 1976;63–1:201–3.
- [31] Johnson RA, Wichern DW. Applied multivariate statistical analysis. 6th ed. New Jersey: Pearson Prentice Hall; 2007.
- [32] López-Camacho E, Terashima-Marín H, Ochoa G, Conant-Pablos SE. Understanding the structure of bin packing problems through principal component analysis. *Int J Prod Econ* 2013;145:488–99.
- [33] Gu F, Hall P, Miles NJ. Performance evaluation for composites based on recycled polypropylene using principal component analysis and cluster analysis. *J Clean Prod* 2016;115:343–53.
- [34] Salah B, Zoheir M, Slimane Z, Jurgen B. Inferential sensor-based adaptive principal components analysis of mould bath level for breakout defect detection and evaluation in continuous casting. *Appl Soft Comput* 2015;34:120–8.
- [35] Ge Z, Song Z, Ding SX, Huang B. Data mining and analytics in the process industry: the role of machine learning. *IEEE Access* 2017;5:20590–616.
- [36] Paiva AP, Paiva EJ, Ferreira JR, Balestrassi PP, Costa SC. A multivariate mean square error optimization of AISI 52100 hardened steel turning. *Int J Adv Manuf Technol* 2009;43:631–43.
- [37] Brito TG, Paiva AP, Ferreira JR, Gomes JHF, Balestrassi PP. A normal boundary intersection approach to multiresponse robust optimization of the surface roughness in end milling process with combined arrays. *Precis Eng* 2014;38:628–38.
- [38] Bhavsar SN, Aravindan S, Rao PV. Investigating material removal rate and surface roughness using multi-objective optimization for focused ion beam (FIB) micro-milling of cemented carbide. *Precis Eng* 2015;40:131–8.
- [39] Ahmadi A, Kaymanesh A, Siano P, Janghorbani M, Nezhad AE, Sarno D. Evaluating the effectiveness of normal boundary intersection method for short-term environmental/economic hydrothermal self-scheduling. *Electr Power Syst Res* 2015;123:192–204.
- [40] Ahmadi A, Aghaei J, Shayanfar HA, Rabiee A. Mixed integer programming of multiobjective hydro-thermal self scheduling. *Appl Soft Comput* 2012;12:2137–46.
- [41] Aghaei J, Amjadi N, Shayanfar HA. Multi-objective electricity market clearing considering dynamic security by lexicographic optimization and augmented epsilon constraint method. *Appl Soft Comput* 2011;11:3846–58.
- [42] Almeida FA, Gomes GF, Paula VR, Correa JE, Paiva AP, Gomes JHF, Turrioni JB. A weighted mean square error approach to the robust optimization of the surface roughness in an AISI 12L14 free-machining steel-turning process. *J Mech Eng* 2018;64:147–56.